AD 805127

COLUMBIA UNIVERSITY

IN THE CITY OF NEW YORK

ELECTRONICS RESEARCH LABORATORIES

632 WEST 125th STREET

NEW YORK, NEW YORK 10027

January 15, 1967

BIREFRINGENCE IN AMORPHOUS SOLIDS WITH APPLICATION TO SOLID LIGHT MODULATORS

TECHNICAL REPORT T-3/321

By

S. Bernstein
J. Minkoff
M. Arm

Prepared for

Director
Advanced Research Projects Agency
Washington, D.C. 20301

and

Electronics Division
Directorate of Engineering Sciences
Air Force Office of Scientific Research
Office of Aerospace Research
U.S. Air Force
Arlington, Virginia 22209

Contract No. AF 49(638)-1478
ARPA Order No. 279

ABSTRACT

The theory of birefringence in a transparent, amorphous solid is developed from fundamental principles in order to obtain a design formulation for spatial light modulators that will operate at 100 MHz center frequency with at least 50 per cent bandwidth. Both longitudinal and shear wave elasto-optical interactions are treated.

Relations for the phase modulation index and the diffracted light intensity and polarization, as functions of the modulator parameters, are presented for the case of normal light incidence. The effect of internal refraction on the first-order peak intensity is then quantitatively examined. From this consideration, a criterion for obtaining maximum optical performance in the modulator is derived.

An analysis of the quartz transducers used to generate the elastic waves in the modulators is presented as an integral part of the design formulation. The effect of lead and indium bonds on transducer response is treated in detail.

AUTHORIZATION

The research described in this report was performed at the Electronics Research Laboratories of Columbia University, within the Electro-Optics Laboratory, M. Arm, Laboratory Supervisor. This report was prepared by S. Bernstein and J. Minkoff.

This project is directed by the Advanced Research Projects Agency of the Department of Defense and is administered by the Air Force Office of Scientific Research under Contract AF 49(638)-1478.

Submitted by:

L. Lambert
Assistant Director

Approved by:

L. H. O'Neill
Professor of Electrical Engineering
Director

TABLE OF CONTENTS

LIST OF FIGURES

LIST OF FIGURES (CONT'D.)

LIST OF FIGURES (CONT'D.)

LIST OF TABLES

I. INTRODUCTION

As part of the continuing effort in the development of electro-optical signal processing techniques for array antennas at the Columbia University Electronics Research Laboratories, a research program on solid light modulators has been initiated to extend the system bandwidths and time-bandwidth products of real-time processors beyond that which is presently available.[1-12]

The program has proceeded along two complementary paths: a detailed theoretical analysis of birefringence in amorphous solids, with attention focused on its application to spatial light modulators, and experimental verification of the theory and determination of the necessary empirical data for optimal system design, so that, ultimately, the feasibility of employing these devices in very high frequency, wide-band processors can be demonstrated.

This report covers the theoretical work performed over the past year and is concerned, specifically, with the modulator design rather than system considerations. In format, it is divided essentially into two parts. In the first part, the theory of birefringence in amorphous solids is derived from crystal optics theory[13] and the elasto-optic interaction theory as developed by Mueller.[14] In the second part, the fundamental theory is then applied to obtain a design formulation for solid light modulators that will operate in a CW mode at 80 and 100 MHz center frequency.

---

[1] For numbered references see Sec. V.

Consideration has been given to both longitudinal and shear wave interactions to indicate the differences in modulator performance that can be expected, and to establish the electrical drive requirements in each case.

The treatment is restricted to fused-silica solid light modulators which are driven by quartz transducers that are bonded to the delay medium with thin bonds of lead or indium.

II. THEORY OF BIREFRINGENCE IN AMORPHOUS SOLIDS

When a beam of light is passed through a stressed, transparant amorphous solid, it becomes birefringent, i.e., it is doubly refracted. The output light is polarized in two specific directions and the polarized components are shifted in phase with respect to the phase of the incident light. The amount of phase shift exhibited by the components, at each point in the solid, is a direct function of the stresses at that point. Hence, if the stresses are zero, the phase shifts will be zero and the output light will remain essentially the same as the incident light. Thus, an amorphous solid is only temporarily double refracting to the extent of the stress distribution within it at any instant of time.

Transparent crystals such as calcite and quartz are also double refractive. However, this is an intrinsic property of these solids and, therefore, exists even though they are unstressed. The explanation for this property is based upon a fundamental assumption of the existence of a permanent state of electrical anisotropy within the crystals. Since the character of the double refraction in crystals is similar, electromagnetically, to that in stressed amorphous solids, the theory developed for the optics of crystals should be applicable to the latter phenomena, if it is assumed that by stressing, the normally electrically isotropic solid is converted into one which is temporarily electrically anisotropic.

In the following treatment the approach will be to develop the electromagnetic theory first, so that the optical effects of the elasto-optic interaction become clear. Once

this is accomplished, attention will be directed to elastic considerations that create an anisotropic state in the amorphous solid. These elastic considerations will then be related to the optics in order to derive the fundamental elasto-optical equations.

A. OPTICAL PHENOMENA IN A TRANSPARENT ANISOTROPIC SOLID

Consider a plane, monochromatic light wave of angular frequency $\omega_L = 2\pi f_L$, propagating in a transparent crystalline solid that is homogeneous, non-conductive, magnetically isotropic and electrically anisotropic. The relationship between the vector amplitudes of the electric vectors, $\bar{D}$ and $\bar{E}$, is then given by,

$$D_k = \sum_{\ell=1}^{3} \epsilon_{k\ell} E_\ell \quad (k = 1,2,3) \tag{1}$$

where D_k, E_ℓ are the amplitude components of the field vectors along the a_k axes of an arbitrary reference frame and $\epsilon_{k\ell}$ are the dielectric constants of the crystal.

Maxwell's equations, under the conditions described above, become:

$$\nabla \times \bar{\mathcal{H}} = \frac{1}{c} \dot{\bar{\mathcal{D}}}$$
$$\nabla \times \bar{\mathcal{E}} = -\frac{1}{c} \dot{\bar{\mathcal{B}}} \tag{2}$$

with the dot over the vectors implying differentiation with respect to time, t.

If the representation of the electromagnetic field vectors, $\bar{\mathcal{H}}, \bar{\mathcal{B}}, \bar{\mathcal{E}}$, and $\bar{\mathcal{D}}$, is of the form,

$$\bar{\mathcal{F}} = \bar{F}e^{i\omega_L[(\frac{n}{c})\bar{r} \cdot \hat{s} - t]},$$

Eq. (2) reduces to

$$\begin{aligned} n\hat{s} \times \bar{H} &= -\bar{D} \\ n\hat{s} \times \bar{E} &= \bar{B} = \mu\bar{H}, \end{aligned} \tag{3}$$

where n is the refractive index in the crystal, defined by

$$n = \frac{c}{v_p}, \tag{4}$$

v_p is the <u>phase</u> velocity of propagation of the light wave, c is the speed of light in vacuum, $\hat{s}$ the unit vector in the direction of light propagation and μ the magnetic permeability which will be taken as equal to one.

Solving Eq. (3) for $\bar{D}$, in terms of $\bar{E}$, gives the fundamental relationship between these vectors in the electrically anisotropic solid,

$$\bar{D} = n^2[\bar{E} - (\bar{E} \cdot \hat{s})\hat{s}]. \tag{5}$$

Note that, in general, $\bar{D}$ will not be parallel to $\bar{E}$ but rotated as shown in Fig. 1. The fact that $\bar{D}$, $\bar{E}$ and $\hat{s}$ lie in the same plane is a consequence of Eq. (3), and $\bar{H} \perp \hat{s}$.

The anisotropy, as expressed by Eq. (1), has a geometrical interpretation which is very helpful in understanding and explaining the optical action in crystalline media. To arrive at this interpretation, consider the expression for the electric energy density,

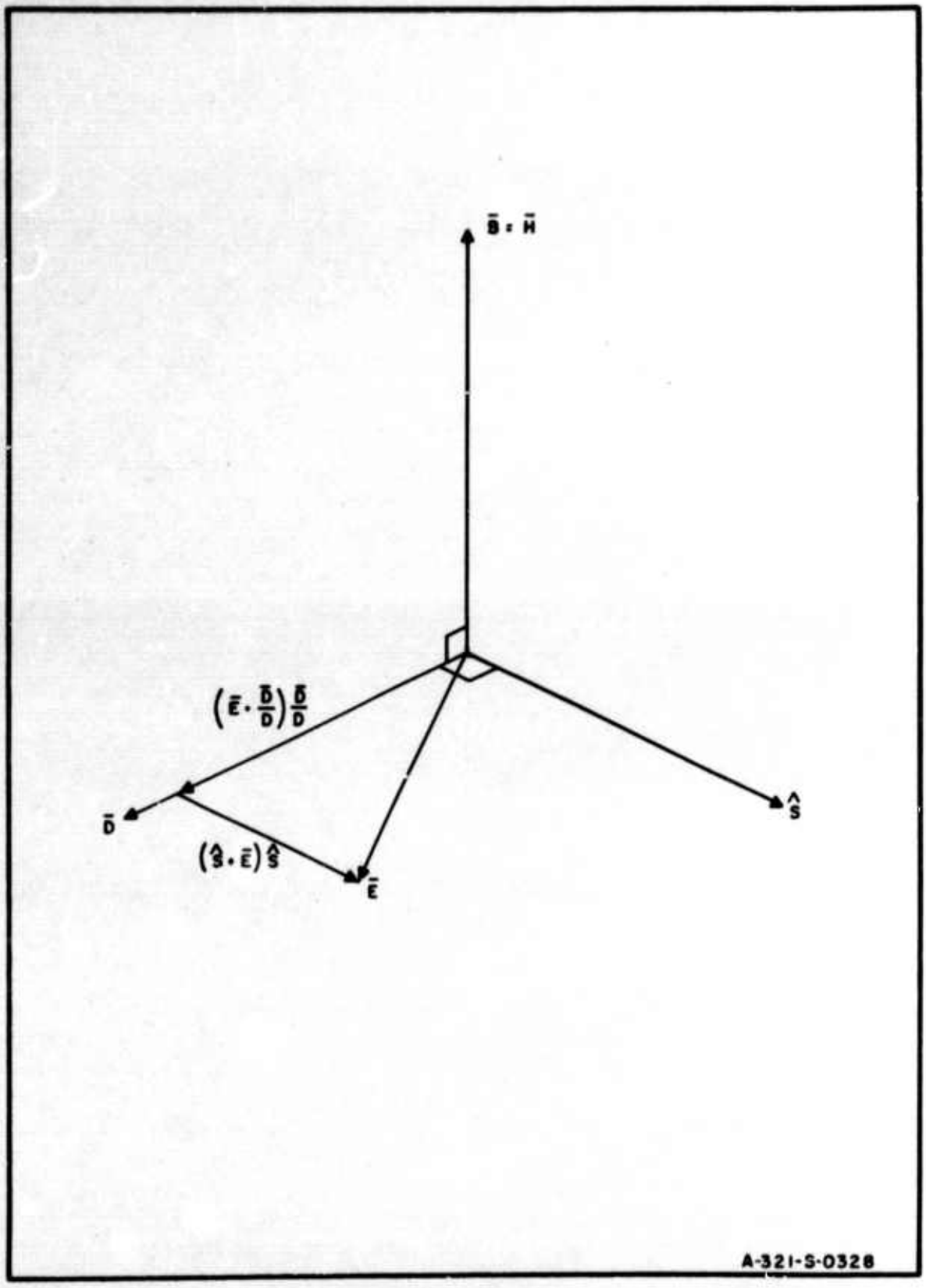

FIG. 1 GEOMETRY OF ELECTROMAGNETIC FIELD VECTORS IN ANISOTROPIC MEDIUM

$$w_e = \frac{1}{8\pi} \sum_{k=1}^{3} \sum_{l=1}^{3} E_k \epsilon_{kl} E_l, \tag{6}$$

where it is assumed that $w_e = (\frac{1}{8\pi})\ \overline{E} \cdot \overline{D}$ is applicable to the anisotropic case. Since w_e is never negative, Eq. (6) is a positive definite quadratic form whose coefficients ϵ_{kl} may be shown to be the components of a symmetric tensor. When this condition exists, three mutually orthogonal axes can always be found along which the $\epsilon_{kl}(k \neq l)$ are identically zero. Then Eq. (6) reduces to,

$$w_e = \frac{1}{8\pi} \sum_{k=1}^{3} \epsilon_k E_k^2, \tag{7}$$

where the ϵ_k are the <u>principal dielectric constants</u> of the medium and the E_k are the components of the electric intensity <u>in the directions of the principal axes</u> of the quadric surface defined by Eq. (6). Along these principal axes, it is seen that

$$D_k = \epsilon_k E_k, \quad (k = 1,2,3) \tag{8}$$

i.e., D_k is parallel to E_k.

Choosing the coordinate reference frame coincident with the principal axes of the quadric, it is possible to determine the geometrical character of the surface by first writing Eq. (7) in the form,

$$8\pi w_e = \kappa = \sum_{k=1}^{3} \frac{D_k^2}{\epsilon_k}, \tag{9}$$

using Eq. (8), and then defining new quantities,

$$x_k = \frac{D_k}{\sqrt{\kappa}}, \quad (k = 1,2,3) \tag{10}$$

so that Eq. (9) becomes

$$\sum_{k=1}^{3} \frac{x_k^2}{\epsilon_k} = 1. \tag{11}$$

This is recognized as the equation of an ellipsoid whose semi-axes have lengths equal to $\sqrt{\epsilon_k}$. Thus, the electrical anisotropy of the crystalline medium at every point is expressible in terms of an index ellipsoid whose size and orientation is governed by the dielectric properties of the medium. The relationship between the index ellipsoid and the optical effects will now be considered.

Solving Eq. (5) for E_k exclusively, by applying Eq. (8), gives

$$E_k = \frac{n^2(\bar{E} \cdot \hat{s})}{n^2 - \epsilon_k} s_k, \quad (k = 1,2,3) \tag{12}$$

where s_k are the components of $\hat{s}$ along the principal axes of the index ellipsoid, taken as a reference frame. Multiplying each E_k of Eq. (12) by its corresponding s_k and summing then yields,

$$\bar{E} \cdot \hat{s} = n^2 \sum_{k=1}^{3} \frac{s_k^2}{n^2 - \epsilon_k} (\bar{E} \cdot \hat{s}) .$$

Hence,

$$\sum_{k=1}^{3} \frac{s_k^2}{n^2 - \epsilon_k} = \frac{1}{n^2} .$$

If this equation is first multiplied through by n^2, and $\hat{s} \cdot \hat{s} = 1$ is subtracted from both sides, there results

$$\sum_{k=1}^{3} \left[\frac{n^2 s_k^2}{n^2 - \epsilon_k} - s_k^2 \right] = \sum_{k=1}^{3} \frac{\epsilon_k}{n^2 - \epsilon_k} s_k^2 = \sum_{k=1}^{3} \frac{s_k^2}{\frac{1}{n^2} - \frac{1}{\epsilon_k}} = 0.$$

Applying Eq. (4) to eliminate n in the last expression, and defining the <u>principal velocities of propagation</u> as

$$v_k = \frac{c}{\sqrt{\epsilon_k}} , \quad (k = 1,2,3) \tag{13}$$

reduces that expression to,

$$\sum_{k=1}^{3} \frac{s_k^2}{v_p^2 - v_k^2} = 0 , \tag{14}$$

which is <u>Fresnel's equation of wave normals</u>. This equation permits the determination of the phase velocity of the light wave in the medium, once the principal dielectric constants and the direction of propagation of the light are known.

In general, there will be two independent solutions for v_p given by the Fresnel equation. Hence, a linearly polarized plane wave incident on an electrically anisotropic medium will be split into two linearly polarized components that

travel with different velocities, v_{p_1} and v_{p_2}, and are oriented according to the resultant of the electric intensity components given by Eq. (12), when it is written in the form

$$E_k = \frac{v_k^2}{v_k^2 - v_p^2} (\bar{E} \cdot \hat{s}) s_k, \quad (k = 1,2,3).$$

The two polarization directions and phase velocities are related to the index ellipsoid in the following manner. Assuming an arbitrary direction of propagation of the incident light wave, specified by the unit vector $\hat{s}$, the plane normal to $\hat{s}$, containing $\bar{D}$, will intersect an index ellipsoid of the medium in an ellipse as shown in Fig. 2. The radius vector $\bar{r}$, from 0 to any point on the ellipse can be described by,

$$r^2 = \sum_{k=1}^{3} x_k^2, \qquad (15)$$

where each x_k must satisfy Eq. (11) and, using Eq. (10), the relation

$$\bar{D} \cdot \hat{s} = \sum_{k=1}^{3} x_k s_k = 0 \ , \qquad (16)$$

simultaneously. At four points along the ellipse this radius vector will be an extremum. Obviously, these points define the axes of symmetry of the section, which are perpendicular to each other. If it can now be shown that when Eq. (5) applies, $\bar{r}$ is an extremum of the <u>index ellipse</u> given by

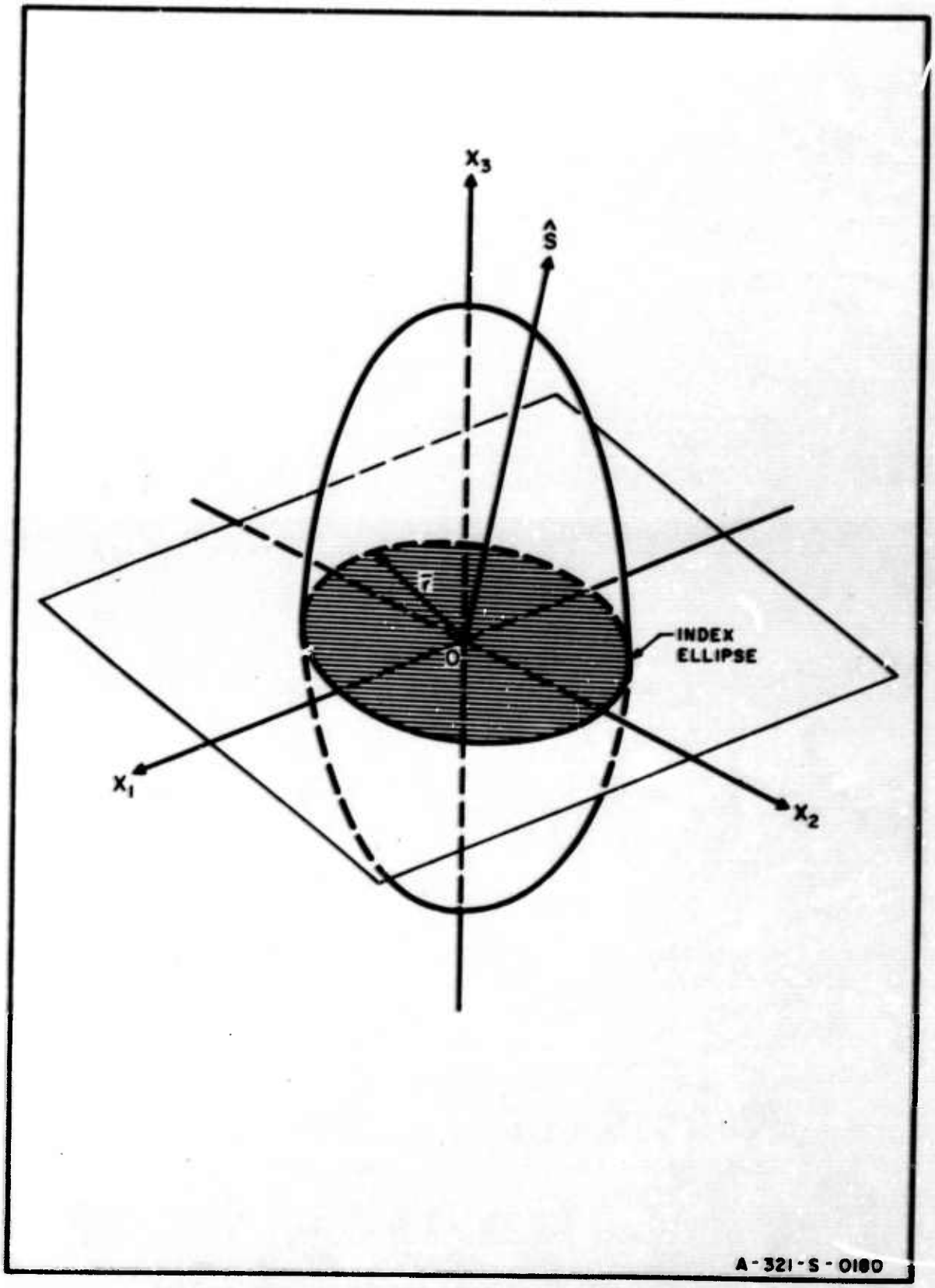

FIG. 2 ELLIPSE FORMED BY INTERSECTION OF PLANE NORMAL TO $\hat{S}$ WITH INDEX ELLIPSOID.

Eq. (15), then the relationship between the light polarization directions in the medium can be clearly established and simply determined for any specific case. Furthermore, it should follow from the nature of the geometry, that the magnitude of $\bar{r}$, when $\bar{r}$ is an extremum, will be proportional to the appropriate phase velocity v_{p_1} or v_{p_2}.

The necessary condition for $\bar{r}$ to be an extremum is obtained by the Lagrange method of undetermined multipliers.[15] In this method the function

$$R = \sum_{k=1}^{3} \left[x_k^2 + 2\alpha x_k s_k + \beta\left(\frac{x_k^2}{\epsilon_k} - 1\right) \right]$$

is formed, noting that the last two terms are identically zero by Eqs. (11) and (16). Hence, R is actually equivalent to r^2, but contains the constraints on $\bar{r}$ in the terms having the, as yet, undetermined multipliers α and β.

If the derivative of R is now taken with respect to x_k and set equal to zero, R and, therefore, $\bar{r}$ will be an extremum. Performing the differentiation,

$$\frac{\partial R}{\partial x_k} = \left(1 + \frac{\beta}{\epsilon_k}\right) x_k + \alpha s_k = 0, \quad (k = 1,2,3) \tag{17}$$

and α and β can be determined by the following simple considerations.

Multiplying Eq. (17) by x_k and summing over k results in

$$\sum_{k=1}^{3}\left[(1+\frac{\beta}{\epsilon_k})x_k^2+\alpha x_k s_k\right]=\sum_{k=1}^{3}\left[x_k^2+\beta\frac{x_k^2}{\epsilon_k}\right]=0,$$

since $\sum_{k=1}^{3} x_k s_k = 0$ by Eq. (16). Applying Eqs. (11) and (15) to the remaining expression then yields,

$$\beta = -r^2. \tag{18}$$

On the other hand, multiplying Eq. (17) by s_k and again summing over k gives immediately,

$$\sum_{k=1}^{3}\left[(1+\frac{\beta}{\epsilon_k})x_k s_k+\alpha s_k^2\right]=\sum_{k=1}^{3}\left[-r^2\frac{x_k s_k}{\epsilon_k}+\alpha\right]=0,$$

using Eq. (18). Hence,

$$\alpha = r^2\sum_{k=1}^{3}\frac{x_k s_k}{\epsilon_k}. \tag{19}$$

Upon substitution of Eqs. (18) and (19) into Eq. (17) the condition that the x_k must satisfy can be written in terms of known parameters and reduced to a form that directly relates to the optical problem. Thus,

$$(1-\frac{r^2}{\epsilon_k})x_k + r^2 s_k\sum_{\ell=1}^{3}\frac{x_\ell s_\ell}{\epsilon_\ell}=0 \quad (k=1,2,3)$$

is the condition that insures that $\bar{r}$ is an extremum of the index ellipse.

To transform this equation into electromagnetic terms it will be recalled that

$$x_k = \frac{D_k}{\sqrt{\kappa}} = \frac{\epsilon_k E_k}{\sqrt{\kappa}},$$

by Eqs. (8) and (10). Substituting for x_k then gives

$$(1 - \frac{r^2}{\epsilon_k}\frac{D_k}{\sqrt{\kappa}} + r^2 s_k \sum_{\ell=1}^{3} \frac{E_\ell}{\sqrt{\kappa}} s_\ell = 0, \quad (k = 1,2,3) \tag{20}$$

but

$$r^2 = \frac{\bar{D} \cdot \bar{D}}{\kappa} = \frac{D^2}{8\pi w_e} = \frac{D^2}{\bar{E} \cdot \bar{D}}$$

by Eqs. (6), (9), (10) and (15). Hence, Eq. (20) becomes

$$(1 - \frac{D^2}{\epsilon_k \bar{E} \cdot \bar{D}})D_k + \frac{D^2 s_k}{\bar{E} \cdot \bar{D}} \sum_{\ell=1}^{3} E_\ell s_\ell = 0. \tag{21}$$

Now, final reduction may be effected by noting that Eq. (5) can be written as

$$\frac{\bar{D}}{n^2} = \bar{E} - (\bar{E} \cdot \hat{s})\hat{s} = (\bar{E} \cdot \frac{\bar{D}}{D})(\frac{\bar{D}}{D}),$$

with reference to Fig. 1. Therefore,

$$n^2 = \frac{\bar{D}}{(\bar{E} \cdot \frac{\bar{D}}{D})(\frac{\bar{D}}{D})} = \frac{D^2}{\bar{E} \cdot \bar{D}} = r^2, \tag{22}$$

and Eq. (21) simplifies to

$$(1 - \frac{n^2}{\epsilon_k})D_k + n^2 s_k \sum_{\ell=1}^{3} E_\ell s_\ell = 0,$$

or

$$D_k = n^2[E_k - (\bar{E} \cdot \hat{s})s_k], \quad (k = 1,2,3)$$

which is just the component form of Eq. (5). Thus, when Eq. (5) applies, the light waves will be polarized in the directions of the principal axes of the index ellipse and, therefore, always at right angles to each other.

The relationship between the magnitude of $\bar{r}$ and the phase velocity v_p is established by Eqs. (4) and (22), giving

$$v_p = \frac{c}{r} . \tag{23}$$

Note that in an electrically isotropic medium, where the index ellipse degenerates into a circle, the two phase velocities are equal, precluding the necessary condition for double refraction.

Summarizing these results, it is seen that the two monochromatic plane light waves that propagate in an electrically anisotropic medium are linearly polarized at right angles to each other, with their directions of polarization coincident with the principal axes of the index ellipse formed by the intersection of the plane normal to the direction of light propagation and the index ellipsoid of the medium. The phase velocities of the waves are inversely

proportional to the half-lengths of the principal axes of the index ellipse. When the half-lengths are equal, the net birefringence is zero. This condition occurs only when the light is propagating either along the optic axis of a crystal or in an electrically isotropic medium.

B. ELASTIC PROPERTIES OF AMORPHOUS SOLIDS

As previously indicated, an amorphous solid must be stressed in order to create the conditions for birefringence. The primary mechanisms, however, that transform the internal structure of the material from the isotropic to the anisotropic state are the elastic deformations or strains induced by the stress.[16] It is therefore natural, then, to develop the subsequent elasto-optic interaction theory in these terms, rather than in terms of the stresses, in order to provide a true picture of the phenomena. Once the formulation is complete, the conversion to the more useful stress form is easily accomplished by means of the stress-strain relationship,

$$T_k = \sum_{\ell=1}^{6} C_{k\ell} S_\ell \, , (k = 1 \text{ to } 6) \qquad (24)$$

where T_k are the components of stress, S_ℓ the components of strain and $C_{k\ell}$ the elastic constants of the medium.

The complete symmetry of the amorphous solid's internal structure reduces the number of independent elastic constants to two, C_{11} and C_{12}. However, a shear constant, C_{44}, exists, which may be expressed in terms of the independent constants as,

$$C_{44} = \frac{C_{11} - C_{12}}{2} \, . \qquad (25)$$

The matrix of the elastic constants for this type of material is then

$$\begin{bmatrix} C_{11} & C_{12} & C_{12} & 0 & 0 & 0 \\ C_{12} & C_{11} & C_{12} & 0 & 0 & 0 \\ C_{12} & C_{12} & C_{11} & 0 & 0 & 0 \\ 0 & 0 & 0 & C_{44} & 0 & 0 \\ 0 & 0 & 0 & 0 & C_{44} & 0 \\ 0 & 0 & 0 & 0 & 0 & C_{44} \end{bmatrix} \tag{26}$$

with no coupling between normal and shear components.

Consider now an initially strain-free amorphous solid in the form of a plate whose major faces are parallel to the x_1x_2-plane, as shown in Fig. 3. The light wave propagates in the $-x_3$-direction and the elastic wave is constrained to propagate in the x_1x_2-plane only. The dimensions of the plate are assumed to be large enough, compared to the elastic wavelength, so that the wave propagates freely in the medium, i.e., uninfluenced by the boundaries.

Let $\hat{k}$ be the unit vector specifying the direction of elastic wave propagation in the x_1x_2-plane, and let ϕ be the angle this vector makes with the x_1-axis.

If the elastic wave is a plane, harmonic wave of frequency f_e, then the elastic displacement at a point P in the plate is given by

$$\bar{u} = \bar{U} \cos(\omega_e t - \bar{k} \cdot \bar{r}) \tag{27}$$

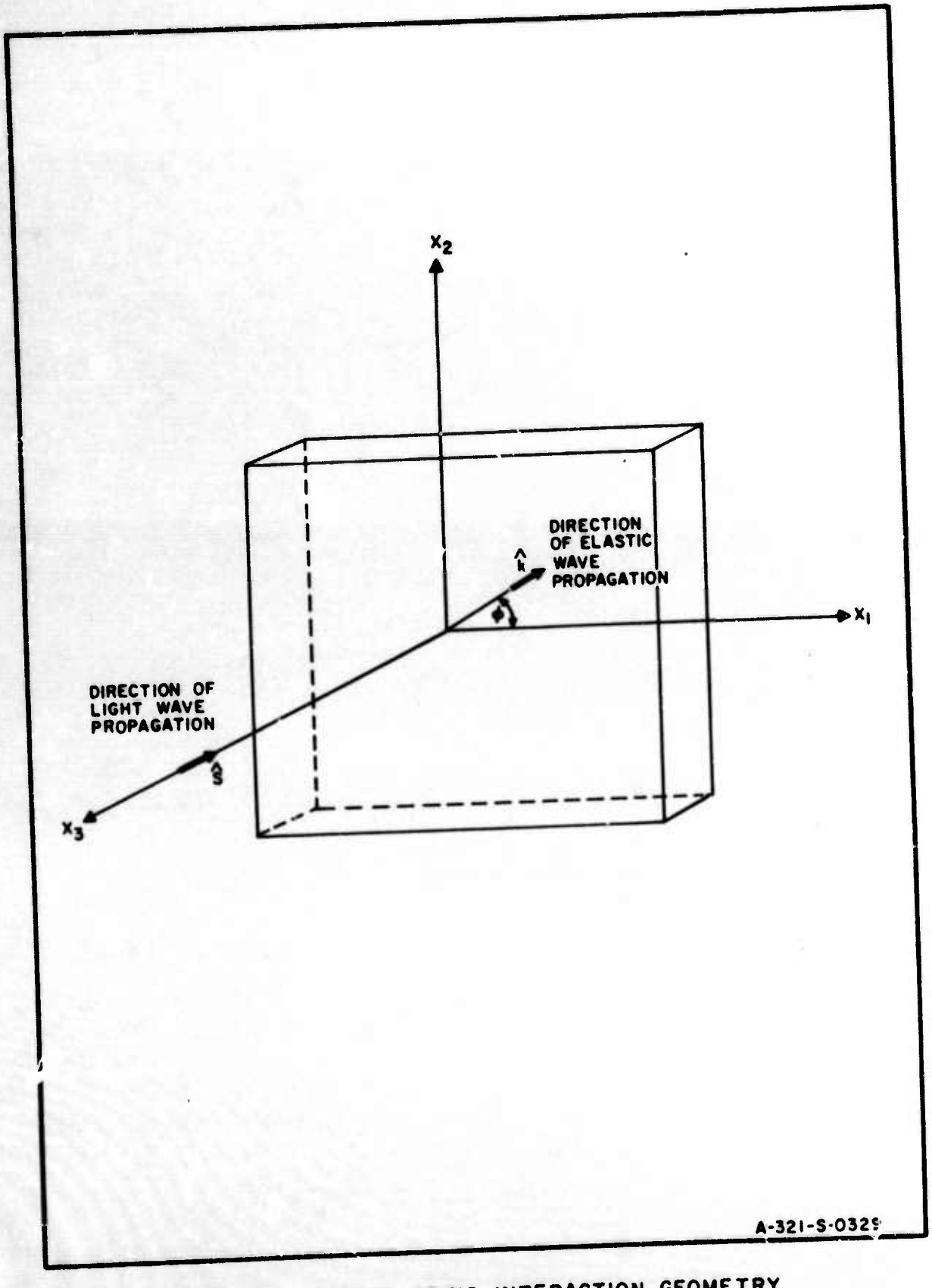

FIG. 3 ELASTO-OPTIC INTERACTION GEOMETRY

where $\bar{U}$ is the displacement amplitude, $\omega_e = 2\pi f_e$, $\bar{k} = \frac{2\pi}{\lambda_e}\hat{k}$ is the propagation vector, λ_e is the elastic wavelength, and $\bar{r}$ is the position vector to the point P.

In order for Eq. (27) to represent a true displacement in the elastic medium, it must satisfy the equations of motion, which in their most general form are,[17]

$$\rho \frac{\partial^2 u_k}{\partial t^2} = \sum_{\ell=1}^{3} \delta_{k\ell} \frac{\partial^2 u_\ell}{\partial \xi^2}, \quad (k = 1,2,3) . \tag{28}$$

Here, u_k are the components of $\bar{u}$, ρ the density of the medium, $\delta_{k\ell}$ elastic moduli that are functions of $C_{k\ell}$ and ϕ, and ξ a new variable related to $\bar{k} \cdot \bar{r}$ through

$$\bar{k} \cdot \bar{r} = \frac{2\pi}{\lambda_e} \hat{k} \cdot \bar{r} = \frac{2\pi}{\lambda_e} \xi . \tag{29}$$

The elastic moduli, $\delta_{k\ell}$, for an amorphous solid supporting a wave propagating in the x_1x_2-plane only, are:

$$\delta_{11} = \alpha^2 C_{11} + \beta^2 C_{44}$$

$$\delta_{12} = \delta_{21} = \alpha\beta(C_{12} + C_{44})$$

$$\delta_{13} = \delta_{31} = 0$$

$$\delta_{22} = \alpha^2 C_{44} + \beta^2 C_{11}$$

$$\delta_{23} = \delta_{32} = 0$$

$$\delta_{33} = C_{44}$$

where $\alpha = \cos\phi$, $\beta = \sin\phi$ are the direction cosines of $\hat{k}$ with respect to the x_1, x_2 axes.

Substituting these moduli into Eq. (28) defines the specific equations of motion relevant to the geometry of Fig. 3,

$$\rho \frac{\partial^2 u_1}{\partial t^2} = (\alpha^2 C_{11} + \beta^2 C_{44}) \frac{\partial^2 u_1}{\partial \xi^2} + \alpha\beta (C_{12} + C_{44}) \frac{\partial^2 u_2}{\partial \xi^2}$$

$$\rho \frac{\partial^2 u_2}{\partial t^2} = \alpha\beta (C_{12} + C_{44}) \frac{\partial^2 u_1}{\partial \xi^2} + (\alpha^2 C_{44} + \beta^2 C_{11}) \frac{\partial^2 u_2}{\partial \xi^2} \qquad (30)$$

$$\rho \frac{\partial^2 u_3}{\partial t^2} = C_{44} \frac{\partial^2 u_3}{\partial \xi^2} \quad .$$

If Eq. (27) is now written in component form as,

$$u_k = U_k \cos(\omega_e t - \frac{2\pi}{\lambda_e}\xi), \quad (k = 1,2,3)$$

using Eq. (29), and the operations indicated in Eq. (30) are performed, there results the following set of conditions on the U_k:

$$[(\alpha^2 C_{11} + \beta^2 C_{44}) - \rho v_e^2] U_1 + \alpha\beta (C_{12} + C_{44}) U_2 = 0$$

$$\alpha\beta (C_{12} + C_{44}) U_1 + [(\alpha^2 C_{44} + \beta^2 C_{11}) - \rho v_e^2] U_2 = 0 \qquad (31)$$

$$(C_{44} - \rho v_e^2) U_3 = 0$$

where v_e is the speed of propagation of the elastic wave.

These conditions allow the determination of the speed of propagation and the relationships between the U_k. In the simplest case, letting $U_1 = U_2 = 0$ and $U_3 \neq 0$, the last of Eq. (31) yields,

$$v_e = \sqrt{\frac{c_{44}}{\rho}} \equiv v_e^T.$$

Since the direction of propagation is in the x_1x_2-plane, U_3 is transverse to this direction and thus represents the propagation of a pure transverse wave whose displacements are parallel to the direction of light propagation, $\hat{s}$.

When $U_1, U_2 \neq 0$ and $U_3 = 0$, the displacements are confined to the x_1x_2-plane and the relationship between them can be obtained by noting that unique values of v_e will exist only when the determinant of the coefficients is equal to zero. Setting the determinant equal to zero, and solving for v_e, gives two distinct solutions to the determinantal equation,

$$v_{e_1} = \sqrt{\frac{c_{11}}{\rho}}$$

$$v_{e_2} = \sqrt{\frac{c_{44}}{\rho}} .$$

By substituting these expressions back into the first of Eq. (31) it is found that,

$$U_2 = \frac{\beta}{\alpha} U_1$$

with $v_e = v_{e_1}$, and

$$U_2 = -\frac{\alpha}{\beta} U_1$$

with $v_e = v_{e_2}$. Therefore, by a simple geometric interpretation of these relationships, it is established that v_{e_1} is the speed of propagation of a longitudinal wave, while v_{e_2} is the propagation speed for a transverse wave whose displacements are always perpendicular to those of the longitudinal wave. Hence,

$$v_e^L = \sqrt{\frac{C_{11}}{\rho}}, \quad v_e^T = \sqrt{\frac{C_{44}}{\rho}} \tag{32}$$

and it may be concluded that an amorphous solid will support two types of waves simultaneously, a pure L-wave with displacements in the direction of $\hat{k}$ and a pure T-wave with displacements normal to $\hat{k}$.

C. THE ELASTO-OPTIC INTERACTION

In the strain-free plate of Fig. 3, as already noted, the index ellipsoid, Eq. (11), at any point P is degenerate to a sphere because the medium is optically (i.e., electrically) isotropic. The radius of this sphere is equal to $\sqrt{\epsilon}$, where ϵ is the characteristic dielectric constant. Hence, by Eqs. (11) and (22), the expression for the circular section in the x_1x_2-plane may be written in the form,

$$\frac{x_1^2}{\epsilon} + \frac{x_2^2}{\epsilon} = \frac{x_1^2}{n_o^2} + \frac{x_2^2}{n_o^2} = 1. \tag{33}$$

When an elastic wave is propagating in the plate, the induced strains modify the dielectric properties of the medium so that it becomes birefringent. This birefringent state is expressed geometrically by distorting the circular section into an ellipse which, in general, has its principal axes rotated through an angle θ, as shown in Fig. 4. The equation of the index ellipse is

$$a_{11}x_1^2 + a_{22}x_2^2 + 2a_{12}x_1x_2 = 1 , \tag{34}$$

where the a_{kl} are known as polarization constants. They will be shown later to be reciprocal to the squares of the refractive indices in the index ellipse.

The fundamental assumption of the linear theory of birefringence in solids is that the difference between the polarization constants of Eq. (34) and the corresponding reciprocals of the square of the characteristic refractive index of Eq. (33) is a linear combination of the components of strain. In general, there will be six equations in six variables. However, because the constants in the linear combination display the same matrix pattern as the elastic constants in Eq. (25), the number of terms in these elasto-optic equations will reduce to:

$$\begin{aligned} a_{11} - \frac{1}{n_o^2} &= p_{11}S_{11} + p_{12}S_{22} + p_{12}S_{33} \\ a_{22} - \frac{1}{n_o^2} &= p_{12}S_{11} + p_{11}S_{22} + p_{12}S_{33} \\ a_{12} &= p_{44}S_{12}, \end{aligned} \tag{35}$$

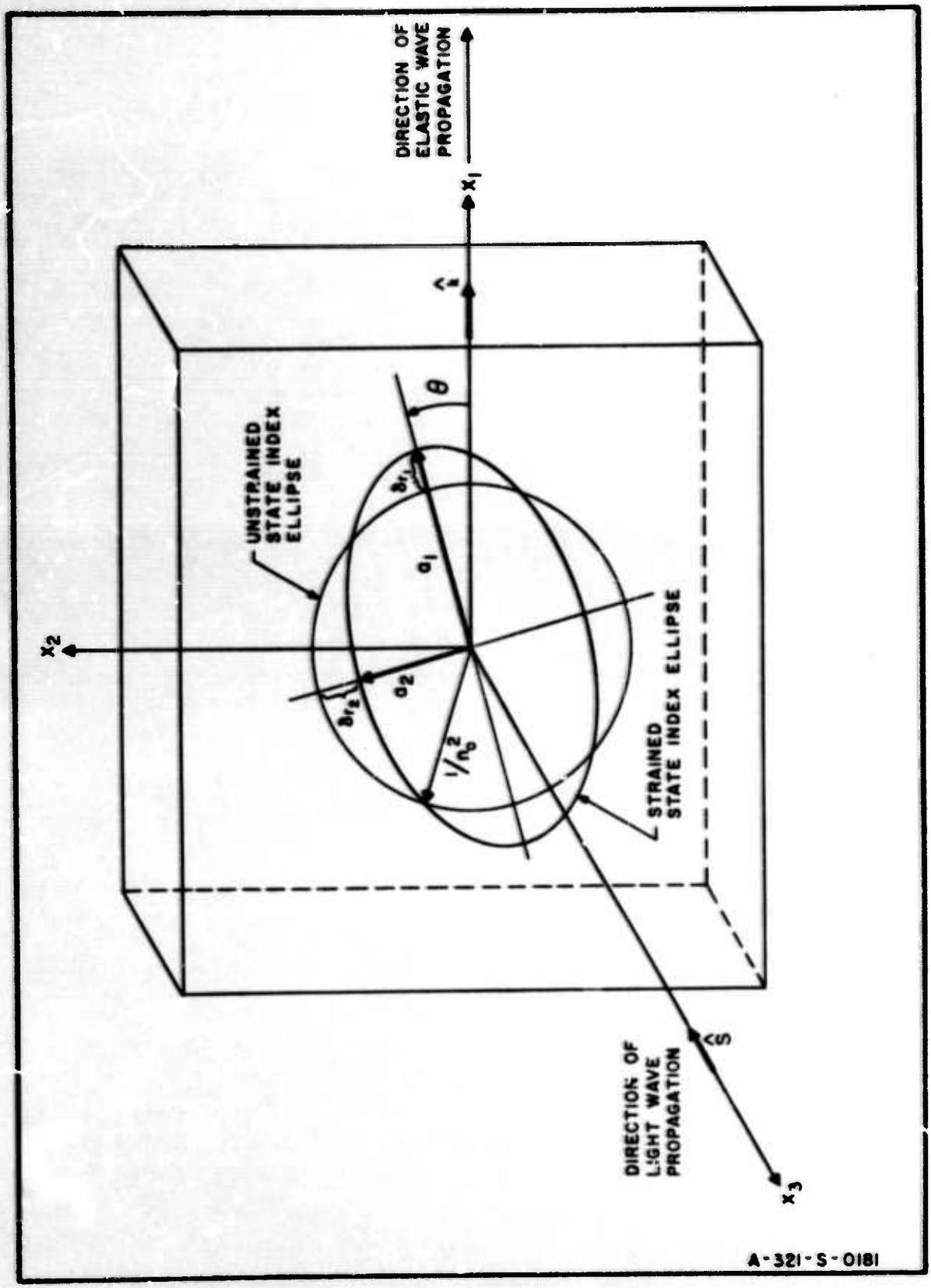

FIG. 4 PROPERTIES OF INDEX ELLIPSES IN STRAINED AND UNSTRAINED STATES FOR ELASTIC WAVE PROPAGATION IN X_1- DIRECTION AND LIGHT WAVE PROPAGATION IN X_3- DIRECTION .

where consideration has been given to the fact that variations in the index ellipsoid in planes normal to the $x_1 x_2$-plane, for the geometry of Fig. 4, have no effect upon the birefringence.

The $p_{k\ell}$ in Eq. (35) are the Pockel elasto-optic constants for an amorphous solid and the $S_{k\ell}$ are the strain components. The elasto-optic constant p_{44} is not an independent constant, but is related to the other two by an expression similar to Eq. (25),

$$p_{44} = \frac{p_{11} - p_{12}}{2} . \tag{36}$$

This is due to the effects of symmetry, where it can be shown that in an amorphous medium only two independent constants are necessary to describe the elasto-optic behavior.

The components of strain in Eq. (35) are functions of the displacement components according to the following formulas from elementary elasticity theory:

$$\begin{aligned} S_{kk} &= \frac{\partial u_k}{\partial x_k} \quad (k = 1,2,3) \\ S_{k\ell} &= \frac{\partial u_k}{\partial x_\ell} + \frac{\partial u_\ell}{\partial x_k}, \ (k \neq \ell), \end{aligned} \tag{37}$$

with the x_k here as spatial coordinates. In these terms, using Eq. (27):

$$S_{11} = \frac{2\pi}{\lambda_e} U_1 \cos\phi \sin(\omega_e t - \bar{k} \cdot \bar{r})$$

$$S_{22} = \frac{2\pi}{\lambda_e} U_2 \sin\phi \sin(\omega_e t - \bar{k} \cdot \bar{r}) \qquad (38)$$

$$S_{33} = 0$$

$$S_{12} = \frac{2\pi}{\lambda_e} (U_1 \sin\phi + U_2 \cos\phi) \sin(\omega_e t - \bar{k} \cdot \bar{r}) .$$

Equation (38) may be put into a more useful form by converting it to functions of U_L and U_T, i.e., longitudinal and transverse wave displacements (Fig. 5). There results:

L-Waves

$$S_{11} = \frac{2\pi}{\lambda_{eL}} U_L \cos^2\phi \sin(\omega_e t - \bar{k} \cdot \bar{r})$$

$$S_{22} = \frac{2\pi}{\lambda_{eL}} U_L \sin^2\phi \sin(\omega_e t - \bar{k} \cdot \bar{r}) \qquad (39)$$

$$S_{12} = \frac{2\pi}{\lambda_{eL}} U_L \sin 2\phi \sin(\omega_e t - \bar{k} \cdot \bar{r}) .$$

T-Waves

$$S_{11} = \frac{-2\pi}{\lambda_{eT}} U_T \sin\phi \cos\phi \sin(\omega_e t - \bar{k} \cdot \bar{r})$$

$$S_{22} = \frac{2\pi}{\lambda_{eT}} U_T \sin\phi \cos\phi \sin(\omega_e t - \bar{k} \cdot \bar{r}) \qquad (40)$$

$$S_{12} = \frac{2\pi}{\lambda_{eT}} U_T \cos 2\phi \sin(\omega_e t - \bar{k} \cdot \bar{r}) .$$

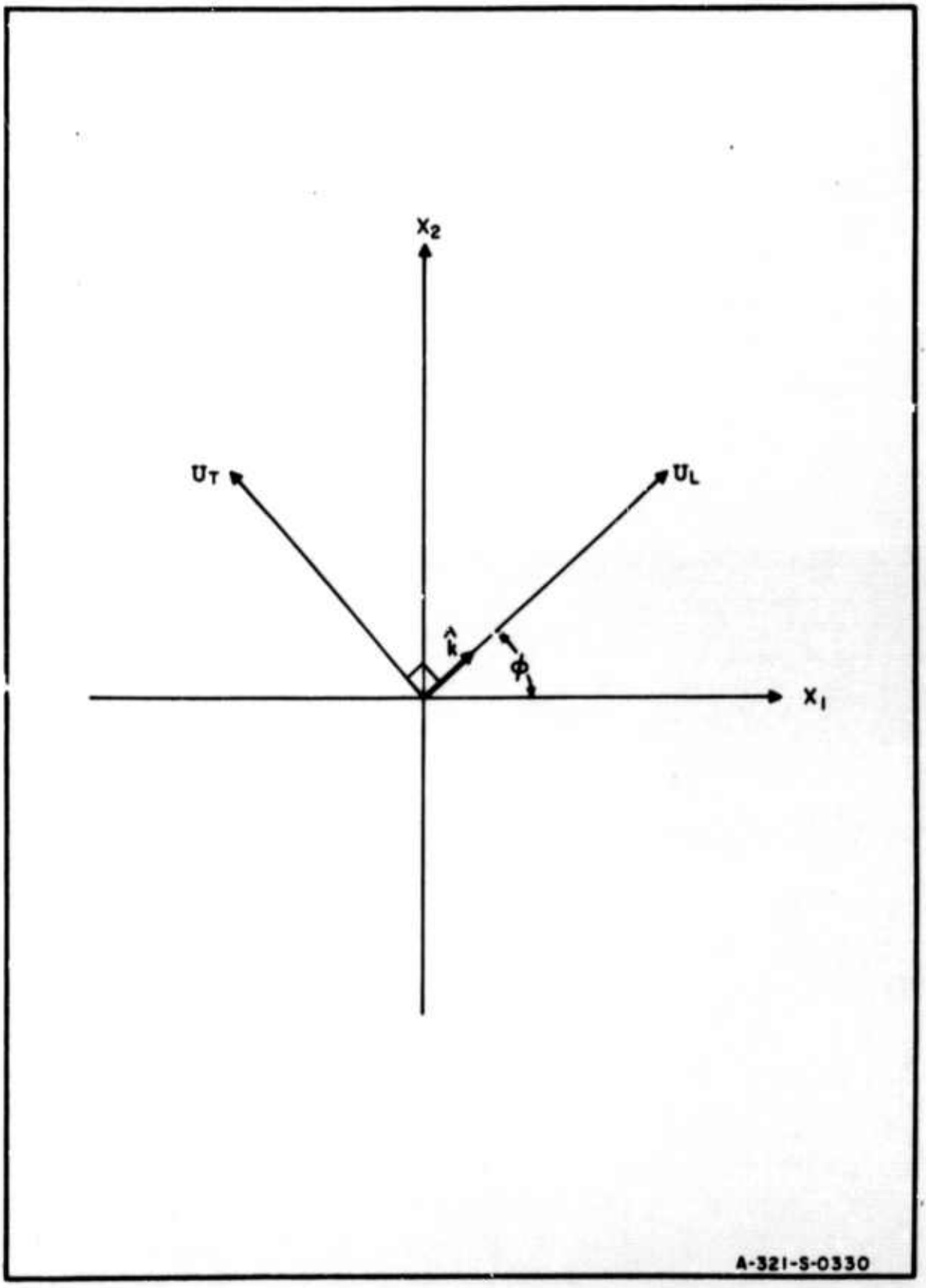

FIG. 5 GEOMETRY FOR TRANSFORMATION OF ELASTIC DISPLACEMENT COMPONENTS

With the establishment of the elasto-optic equations and the strains that are pertinent to Fig. 4, it is now possible to proceed directly to a determination of the angle θ and the refractive index changes along the principal axes of the index ellipse.

The angle θ is obtained by making a coordinate transformation from the x_1, x_2 axes to the x_1', x_2' axes which are coincident with the principal axes. The transformation equations

$$x_1' = x_1 \cos\theta + x_2 \sin\theta$$

$$x_2' = -x_1 \sin\theta + x_2 \cos\theta$$

are first substituted into the equation

$$a_1 x_1'^2 + a_2 x_2'^2 = a_{11} x_1^2 + a_{22} x_2^2 + 2a_{12} x_1 x_2$$

which describes the invariance of the index ellipse to such a transformation. Then, the coefficients of like variables are equated to yield,

$$\begin{aligned} a_{11} &= a_1 \cos^2\theta + a_2 \sin^2\theta \\ a_{22} &= a_1 \sin^2\theta + a_2 \cos^2\theta \\ 2a_{12} &= (a_1 - a_2) \sin 2\theta \ . \end{aligned} \tag{41}$$

If the second of Eq. (41) is now subtracted from the first, and the third divided by $\sin 2\theta$,

$$a_1 - a_2 = \frac{a_{11} - a_{22}}{\cos 2\theta} = \frac{2a_{12}}{\sin 2\theta} .$$

Hence, the orientation of the index ellipse is governed by,

$$\tan 2\theta = \frac{2a_{12}}{a_{11} - a_{22}} . \tag{42}$$

Substitution of Eqs. (39) and (40) into Eq. (35) leads to specific forms of the polarization constants in Eq. (42). Then, θ may be evaluated for both L and T waves. It is found that,

$$\theta_L = \phi \tag{43}$$

and

$$\tan 2\theta_T = - \cot 2\phi .$$

The latter expression can be put into a simpler form by writing it as,

$$\cos 2\theta_T \cos 2\phi + \sin 2\theta_T \sin 2\phi = \cos 2(\theta_T - \phi) = 0,$$

and recognizing that in order to satisfy this equation,

$$2(\theta_T - \phi) = \frac{\pi}{2} .$$

Thus,

$$\theta_T = \phi + \frac{\pi}{4} . \tag{44}$$

The L wave is therefore seen to polarize the light in the $\hat{k}$ direction, and at right angles to this direction. A T wave, on the other hand, splits the incident light into two components that make angles of 45 and 135 deg with the $\hat{k}$ direction. Since Eqs. (43) and (44) are functions of ϕ only, the orientation of the index ellipse is also seen to be the same at every point in the elastic wave field.

Although the orientation of the index ellipse is fixed once the direction of elastic wave propagation is known, the lengths of the principal axes will vary with the variations in strain. Let the change in length of these axes be denoted by,

$$\delta r_1 = a_1 - \frac{1}{n_o^2}$$

$$\delta r_2 = a_2 - \frac{1}{n_o^2} , \qquad (45)$$

as indicated in Fig. 4. Since the phase shifts in the transmitted light are of major interest, it is important to express δr_1 and δr_2 as changes in refractive index, in terms of the elasto-optic properties of the medium and the strains.

Toward this end, it is first noted that,

$$a_1 + a_2 = a_{11} + a_{22}$$

$$a_1 - a_2 = \frac{2a_{12}}{\sin 2\vartheta} ,$$

from Eq. (41). Hence,

$$a_1 = \frac{a_{11} + a_{22}}{2} + \frac{a_{12}}{\sin 2\theta}$$
$$a_2 = \frac{a_{11} + a_{22}}{2} - \frac{a_{12}}{\sin 2\theta} . \qquad (46)$$

If Eq. (35) is now substituted for the polarization constants and the resulting expressions applied to Eq. (45),

$$\delta r_1 = \frac{(p_{11} + p_{12})(S_{11} + S_{12})}{2} + \frac{p_{44} S_{12}}{\sin 2\theta}$$
$$\delta r_2 = \frac{(p_{11} + p_{12})(S_{11} + S_{12})}{2} - \frac{p_{44} S_{12}}{\sin 2\theta} .$$

These formulas can be simplified by forming the sum and difference functions,

$$\delta r_1 + \delta r_2 = (p_{11} + p_{12})(S_{11} + S_{12})$$
$$\delta r_1 - \delta r_2 = \frac{2p_{44} S_{12}}{\sin 2\theta} , \qquad (47)$$

and eliminating the $\sin 2\theta$ as follows.

When Eq. (42) is written in terms of the strain, by substitution of Eq. (35),

$$\tan 2\theta = \frac{2p_{44} S_{12}}{(p_{11} - p_{12})(S_{11} - S_{22})} .$$

This equation has a geometrical interpretation. The numerator is just the altitude of a right triangle whose hypotenuse makes an angle 2θ with the base, or denominator. The length of the hypotenuse is, therefore,

$$h = \sqrt{(p_{11} - p_{12})^2(S_{11} - S_{22})^2 + 4p_{44}^2 S_{12}^2} \quad .$$

Then, the $\sin 2\theta$ must be,

$$\sin 2\theta = \frac{2p_{44} S_{12}}{h} \quad ,$$

and the difference

$$\delta r_1 - \delta r_2 = h = (p_{11} - p_{12})[(S_{11} - S_{22})^2 + S_{12}^2]^{\frac{1}{2}} \quad , \qquad (48)$$

using Eq. (36).

Considering first an L wave propagating in the $\hat{k}$ direction, Eqs. (47) and (48) now allow a unique representation of δr_1 and δr_2, in their simplest form, once the stains are written in terms of the displacement U_L by means of Eq. (39). The sum and difference functions in this case are,

$$\begin{aligned} \delta r_1 + \delta r_2 &= (p_{11} + p_{12})U_L \\ \delta r_1 - \delta r_2 &= (p_{11} - p_{12})U_L \quad , \end{aligned} \qquad (49)$$

neglecting the common multiplicative factor. If $p_{11} > p_{12}$ and S_{12} is of positive sign,* the solutions to Eq. (49) are:

$$\delta r_1 = p_{11} U_L$$

$$\delta r_2 = p_{12} U_L \,. \tag{50}$$

With S_{12} negative, an apparent rotation of the principal axes through 90 deg occurs and,

$$\delta r_1 = p_{12} U_L \qquad \delta r_2 = p_{11} U_L \,.$$

The solutions for a T wave follow just as easily by application of Eq. (40). Here, the sum and difference functions are,

$$\delta r_1 + \delta r_2 = 0$$

$$\delta r_1 - \delta r_2 = \pm (p_{11} - p_{12}) U_T \,.$$

Therefore,

$$\delta r_1 = -\delta r_2 = \pm p_{44} U_T \,. \tag{51}$$

The most useful forms of Eqs. (50) and (51) are obtained when $\phi = 0$, i.e., the elastic wave propagates in the

* The sign of S_{12} is important because $\delta r_1 - \delta r_2 = \frac{2 p_{44} S_{12}}{\sin 2\theta} = h$ is positive or negative depending on the sign of S_{12} when $0 < \theta < \pi/2$ and $p_{44} > 0$.

x_1-direction. Then, Eq. (39) indicates that only $S_{11} \neq 0$, and Eq. (40), that only $S_{12} \neq 0$. Recalling the multiplicative factors implicit in Eqs. (50) and (51), it is seen that these formulas now become:

L-Waves

$$\delta r_1 = p_{11} S_{11}$$
$$\delta r_2 = p_{12} S_{11} \qquad (52)$$

T-Waves

$$\delta r_1 = -\delta r_2 = p_{44} S_{12} \, . \qquad (53)$$

Eqs. (52) and (53) are working equations which will be used exclusively in what follows.

The refractive index changes, corresponding to the changes in length of the principal axes indicated in Eqs. (52) and (53), may be derived by noting the relationship between n and r in Eq. (22) and the forms of Eqs. (33) and (34). It will be recalled that in the development of Eq. (22), the index ellipsoid was given by Eq. (11) which is of the same form as Eq. (33). Therefore, it is concluded that

$$a_1 = \frac{1}{r_1^2} = \frac{1}{n_1^2}$$

$$a_2 = \frac{1}{r_2^2} = \frac{1}{n_2^2}$$

and

$$\delta r_1 = \frac{1}{n_1^2} - \frac{1}{n_o^2}$$
$$\delta r_2 = \frac{1}{n_2^2} - \frac{1}{n_o^2}, \qquad (54)$$

by Eq. (45).

Applying Eq. (54) to Eq. (52) now gives,

$$\frac{(n_o - n_1)(n_o + n_1)}{n_o^2 n_1^2} \approx \frac{2(n_o - n_1)}{n_o^3} = p_{11} S_{11}$$

$$\frac{(n_o - n_2)(n_o + n_2)}{n_o^2 n_2^2} \approx \frac{2(n_o - n_2)}{n_o^3} = p_{12} S_{11}$$

if n_1 and n_2 differ only slightly from n_o. The elasto-optic constants on the right are usually expressed in terms of the so-called Neumann strain-optic constants for isotropic media,

$$p_{11} = \frac{2q}{n_o} \qquad p_{12} = \frac{2p}{n_o} \; ; \qquad (55)$$

hence the above formulas may finally be written as,

$$\delta n_{1L} = -n_o^2 q S_{11}$$
$$\delta n_{2L} = -n_o^2 p S_{11} \qquad (56)$$

where $\delta n_{1,2L} \equiv n_{1,2} - n_o$.

The difference in the refractive index changes in Eq. (52),

$$\delta r_1 - \delta r_2 = \frac{1}{n_1^2} - \frac{1}{n_2^2} \approx \frac{2(n_2 - n_1)}{n_o^3} = (p_{11} - p_{12})S_{11}$$

defines the <u>strain-optic constant</u> <u>b</u> given in the literature,

$$b \equiv \frac{\delta n_{21}}{S_{11}} = \frac{n_2 - n_1}{S_{11}} = n_o^2(q - p) \qquad (57)$$

where $\delta n_{21} \equiv n_2 - n_1$ and Eq. (55) is used. This constant simplifies the expressions for T waves, corresponding to those in Eq. (56).

The development for T waves proceeds in similar fashion to that used for L waves except that Eq. (53) replaces Eq. (52). Thus,

$$n_1 - n_o = -(n_2 - n_o) = \frac{-n_o^3}{2} p_{44} S_{12}.$$

Now, introducing Eqs. (36) and (55) into this equation puts it into the form,

$$n_1 - n_o = -(n_2 - n_o) = -\frac{n_o^2(q - p)}{2} S_{12} = -\frac{b}{2} S_{12}.$$

Hence,

$$\delta n_{1T} = -\delta n_{2T} = -\frac{b}{2} S_{12}. \qquad (58)$$

The conversion of Eqs. (56) and (58) to the stress forms, which will find immediate application in the solid light modulators, is accomplished by first inverting Eq. (24) and expressing the coefficients in terms of the commonly known properties of an isotropic medium. It can be shown that,[18]

$$S_{k\ell} = \left(\frac{1 + \sigma}{E}\right) T_{k\ell} , \qquad (k,\ell = 1,2,3)$$

exactly when $k \neq \ell$ and approximately when $k = \ell$. For practical purposes this equivalency is satisfactory in all cases, with σ the Poisson's ratio and E the modulus of elasticity of the medium.

Upon substitution for the $S_{k\ell}$ in the elasto-optic equations the changes in refractive index are then determined by the formulas:

$$\begin{aligned} \delta n_{1L} &= -\left(\frac{1 + \sigma}{E}\right) n_o^2 q T_{11} \\ \delta n_{2L} &= -\left(\frac{1 + \sigma}{E}\right) n_o^2 p T_{11} , \end{aligned} \qquad (59)$$

and

$$\delta n_{1T} = -\delta n_{2T} = -\frac{B}{2} T_{12} \qquad (60)$$

where B, the <u>stress-optic constant</u>, is defined by

$$B \equiv \left(\frac{1 + \sigma}{E}\right) b = \left(\frac{1 + \sigma}{E}\right) n_o^2 (q - p). \qquad (61)$$

III. OPTICAL DIFFRACTION BY BIREFRINGENT AMORPHOUS SOLIDS

As a result of a stress wave propagating in an amorphous solid it has been shown that refractive index changes will occur in specific planes of polarization, at each point in the stress wave field, to an extent dependent upon the magnitude and direction of the stress at that point.

Obviously, the refractive index changes along the direction of elastic wave propagation will conform to the shape of the traveling wave, as is evident from Eqs. (59) and (60). Thus, in effect, a variable optical transmission grating is created whose configuration is directly related to the character of the stress wave at each instant of time.

If the variations in refractive index are small and the thickness of the medium, in the direction of light propagation, is such that internal bending (internal refraction) can be neglected,* the diffraction effects caused by sinusoidal excitation of the solid can be explained by the simple Raman-Nath theory[14].

Consider the geometry in Fig. 6. The light wave propagates along the x_3-axis in the direction specified by $\hat{s}$. Its $\overline{E}$ vector is polarized at an angle γ with respect to the x_1-axis.

A plane, harmonic elastic wave is assumed to propagate in the x_1x_2-plane, along the x_1-axis, in the direction of $\hat{k}$. It induces an index ellipse whose major axis makes, in general, an angle θ with the x_1-axis.

---

* The effect of internal refraction on the diffraction pattern is discussed in Sec. IV-D.

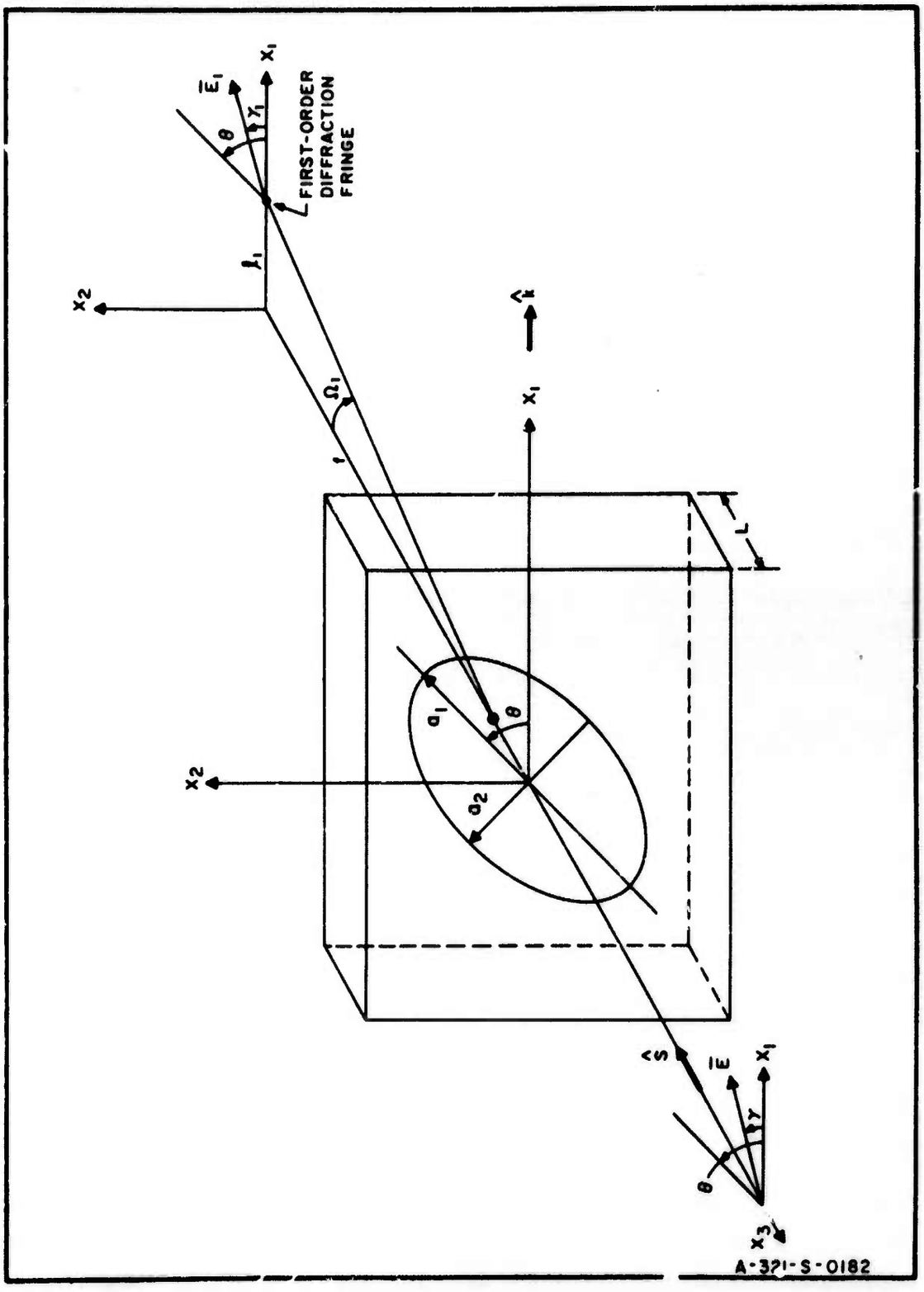

FIG. 6 DIFFRACTION GEOMETRY

When the light wave enters the stressed solid, it splits into two waves which undergo phase shifts with respect to the phase of the incident wave according to,

$$\psi_1 = \frac{2\pi}{\lambda_L} \delta d_1$$

$$\psi_2 = \frac{2\pi}{\lambda_L} \delta d_2,$$

where λ_L is the wavelength of the light and δd is the change in optical path length. The optical path length changes are related to the changes in the refractive indices by the equation,

$$\delta d = L \delta n$$

where L is the geometrical path traversed in the elastic wave field.

Since the elastic wave is harmonic, the amplitudes of the phase shifts are of primary concern. This amplitude is known as the <u>modulation index</u> and is defined by,

$$\psi_m = \frac{2\pi}{\lambda_L} \delta n_m L, \tag{62}$$

with δn_m the maximum change in the refractive index and L now interpreted as the width of the elastic wave field in the direction of $\hat{s}$.

Substituting Eq. (59) into Eq. (62), the modulation indices for an L wave are obtained:

$$\begin{aligned} \psi_{m_{1L}} &= \frac{2\pi}{\lambda_L}\left(\frac{1+\sigma}{E}\right) n_o^2 qL \; T_{mL} \\ \psi_{m_{2L}} &= \frac{2\pi}{\lambda_L}\left(\frac{1+\sigma}{E}\right) n_o^2 pL \; T_{mL} \end{aligned} \tag{63}$$

where T_{mL} is the maximum normal stress T_{11}.

For a T wave,

$$\psi_{m_{1T}} = \psi_{m_{2T}} = \frac{2\pi}{\lambda_L}\left(\frac{B}{2}\right) L T_{ms} \tag{64}$$

upon substitution of Eq. (60), with maximum T_{12} denoted by T_{ms}.

Consider now that the plate of Fig. 6 is uniformly illuminated by a perfectly collimated, linearly polarized beam of light. This beam will be modulated by the elasto-optic interaction in the plate so that, at the output face, its wavefront will vary sinusoidally along the x_1-axis. If a lens of focal length f is interposed between the plate and a screen which is placed in the focal plane of the lens, a diffraction pattern in the form of spots of light will be observed on this screen. The position, with respect to the optical axis, of these spots or diffraction orders, along a line parallel to $\hat{k}$, is given by the formula,*

$$\ell_k = f \tan \Omega_k, \quad (k = 0,1,2,\ldots)$$

where the diffraction angle Ω_k is defined by

$$\sin \Omega_k = k \frac{\lambda_L}{\lambda_e} .$$

When $\lambda_L \ll \lambda_e$, $\sin \Omega_k \approx \Omega_k$ in the lower orders, and

$$\ell_k \simeq f \Omega_k = k f \frac{\lambda_L}{\lambda_e} \tag{65}$$

is sufficiently accurate for most computational purposes.

---

* The diffraction pattern in the direction normal to $\hat{k}$ will be neglected because it is not pertinent to these considerations.

The light intensity distribution in the focal plane of the lens will, in general, depend on the angle γ of the $\bar{E}$ vector, as well as the modulation indices. When $\bar{E}$ is polarized in the direction of one of the principal axes of the index ellipse, Raman-Nath theory indicates that the maximum value of the electric intensity in the k^{th} order will be

$$E_k = EJ_k(\psi_m), \tag{66}$$

where J_k is the k^{th} order Bessel function. Hence, the maximum relative light intensity in the k^{th} diffraction order is*

$$I_{km} = \left(\frac{E_k}{E}\right)^2 = J_k^2(\psi_m).$$

No change in the light polarization will occur in this case because of the initial alignment with the principal axes.

In the more general case where the $\bar{E}$ vector is resolved into birefringence components,

$$\begin{aligned} E_1 &= E\cos(\theta - \gamma) \\ E_2 &= E\sin(\theta - \gamma), \end{aligned} \tag{67}$$

the situation becomes more complex.

First of all, each of the above components gives rise to a diffraction pattern where the maximum electric intensities are,

---

* The relative light intensity distribution in the k^{th} order is of the form $I_k = I_{km}\sin^2x/x^2$. Since the sinc^2x multiplier is of no importance to the present discussion, all formulas for relative intensity will be concerned with the maximum relative intensity only. A complete discussion of the relative light intensity distribution to be expected in the above situation can be found in Ref. 12.

$$E_{1k} = E_1 J_k(\psi_{m1})$$
$$E_{2k} = E_2 J_k(\psi_{m2}). \tag{68}$$

These intensities will be deviated through the same diffraction angle Ω_k, and since they originate from the same incident light, by diffraction on the same elastic wave, the resultant electric intensity in the k^{th} order will then be just their vector sum. Thus, linear polarization is preserved; however, the polarization of the diffracted light can now differ from that of the incident light.

The angle of polarization of the diffracted light is easily determined by considering the geometry in Fig. 7 and Eq. (68). If the ratio

$$\frac{E_{2k}}{E_{1k}} = \tan(\theta - \gamma_k) = \frac{E_2 J_k(\psi_{m2})}{E_1 J_k(\psi_{m1})}$$

is formed and Eq. (67) applied, the polarization angle is given by

$$\tan(\theta - \gamma_k) = \tan(\theta - \gamma) \frac{J_k(\psi_{m2})}{J_k(\psi_{m1})}.$$

For L waves, recalling Eq. (43) with $\phi = 0$,

$$\tan \gamma_k = \tan \gamma \frac{J_k(\psi_{m2})}{J_k(\psi_{m1})}; \tag{69}$$

while for T waves, the angle becomes,

$$\tan(\tfrac{\pi}{4} - \gamma_k) = (-1)^k \tan(\tfrac{\pi}{4} - \gamma), \tag{70}$$

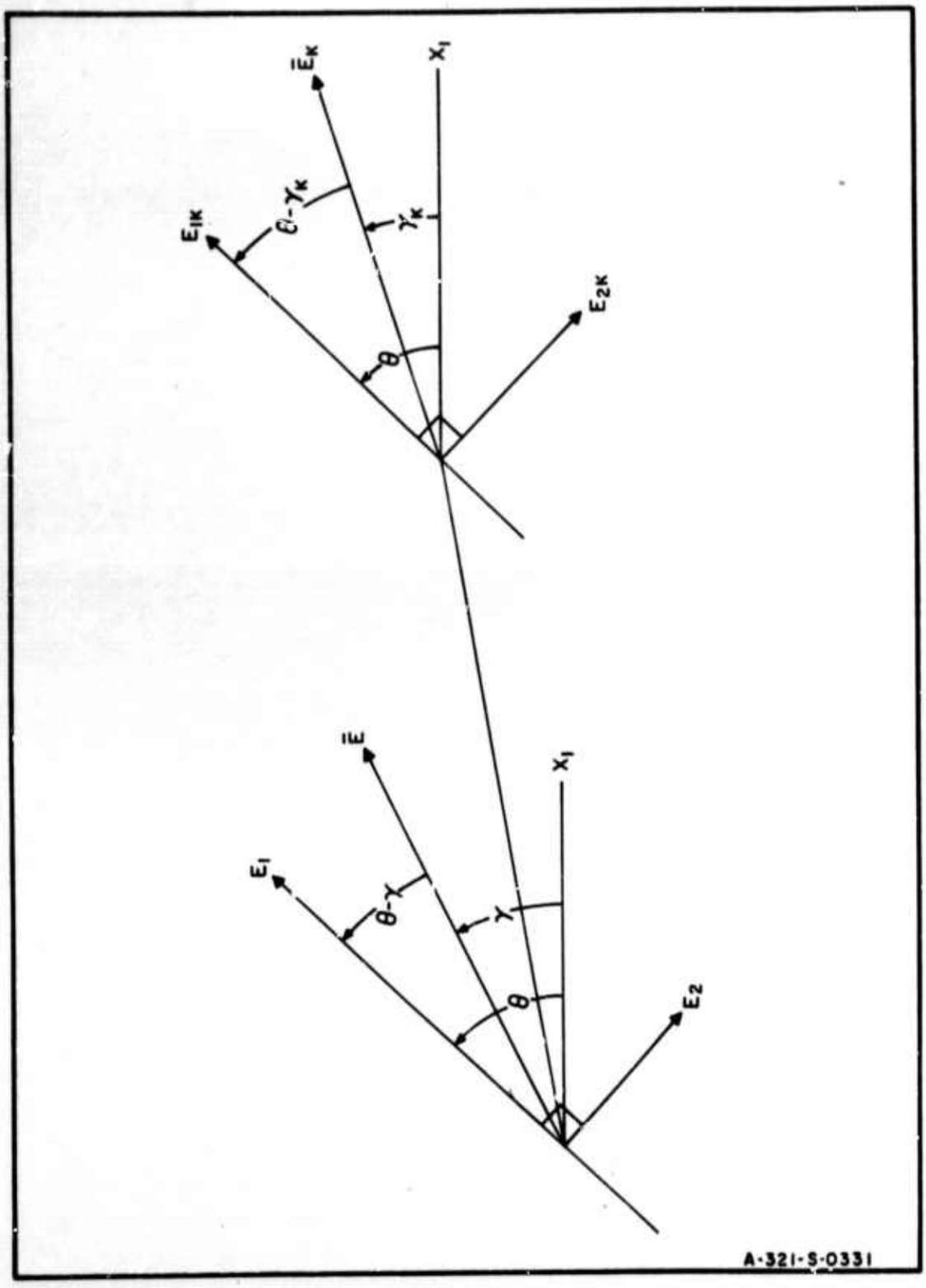

FIG. 7 GEOMETRY FOR DETERMINATION OF γ_K AND I_{Km} FOR ARBITRARY γ

once it is recognized that

$$J_k(\psi_{m_2T}) = J_k(-\psi_{m_1T}) = (-1)^k J(\psi_{m_1T}) ,$$

and Eq. (44) is employed.

The maximum relative light intensity can also be derived immediately by referring to Fig. 7 where

$$I_{km} = \frac{E_{1k}^2 + E_{2k}^2}{E^2} = J_k^2(\psi_{m_1}) \cos^2(\theta - \gamma) + J_k^2(\psi_{m_2}) \sin^2(\theta - \gamma),$$

upon substitution of Eqs. (67) and (68). In the two cases of interest, this equation becomes:

$$I_{kmL} = J_k^2(\psi_{m_1L}) \cos^2\gamma + J_k^2(\psi_{m_2L}) \sin^2\gamma \qquad (71)$$

$$I_{kmT} = J_k^2(\psi_{m_1T}) \qquad (72)$$

where it is seen that for T waves, the maximum relative light intensity in all orders is independent of the polarization of the incident wave.

IV. APPLICATION TO SOLID LIGHT MODULATORS

The results of the theory of birefringence in amorphous solids will now be applied to design considerations for development of a wide-band (50 MHz) solid light modulator operating at a center frequency of 100 MHz. These considerations represent the initial effort in the solid light modulator research program that is presently being conducted at CUERL.

The modulator is essentially an ultrasonic delay line in the form of a plate of very high optical and acoustical quality fused-silica. At one end of the plate, elastic waves are generated by quartz transducers resonating in the fundamental mode. At the other end, a highly efficient absorber attenuates the waves to a level ($>$ 40 dB) where the delay line appears, for all practical purposes, to have an infinite insertion loss. Thus, the elastic waves may be considered, in an analytical sense, as pure traveling waves.

Illumination of the modulator in the experimentation will be provided by a high-intensity gas laser source which emits a beam of light with a 0.6328μ wavelength. The light is highly collimated over the optical aperture by a precision optical system so that a plane wave normally incident on the plate is achieved.[10]

Although the objective of the program, as stated, is the development of a 100 MHz device, the state-of-the-art in fabrication of very high frequency fundamental mode quartz transducers, which meet the program requirements, is such, that this frequency appears to be at the outer limit of the

fabricator's capability. Hence, in what follows, consideration will also be given to 80 MHz modulators since a higher confidence level exists in the fabrication of delay lines at this frequency.

A. SOLID LIGHT MODULATOR CONFIGURATIONS

The simplest solid light modulator is shown in Fig. 8. On the left end of the delay line is the quartz transducer crystal, attached to the line under high pressure and temperature by either an indium or lead bond. This "bond" also serves as the ground electrode for the transducer electrical connections. The positive electrode covers the exposed face of the crystal and determines the transducer size, for only that area of the crystal between the two electrodes will be excited piezoelectrically. This electrode may be a thin vacuum deposited film of indium or a conductive foil supported on a viscous fluid adhesive layer, like vaseline or vacuum grease.

At the right end, a wedge-shaped acoustical absorber is cut into the line. The angle of the wedge depends upon the required amount of attenuation and the achievable energy loss per reflection when the edges of the wedge are coated with lead, a material closely matching the mechanical impedance of fused-silica for shear waves.

By a geometrical analysis, this angle is given by

$$\omega = \frac{180^\circ}{n+1},$$

where n is the total number of reflections in the wedge. If n is even, the analysis indicates that the reflected beam will emerge from the absorber parallel to the inclined

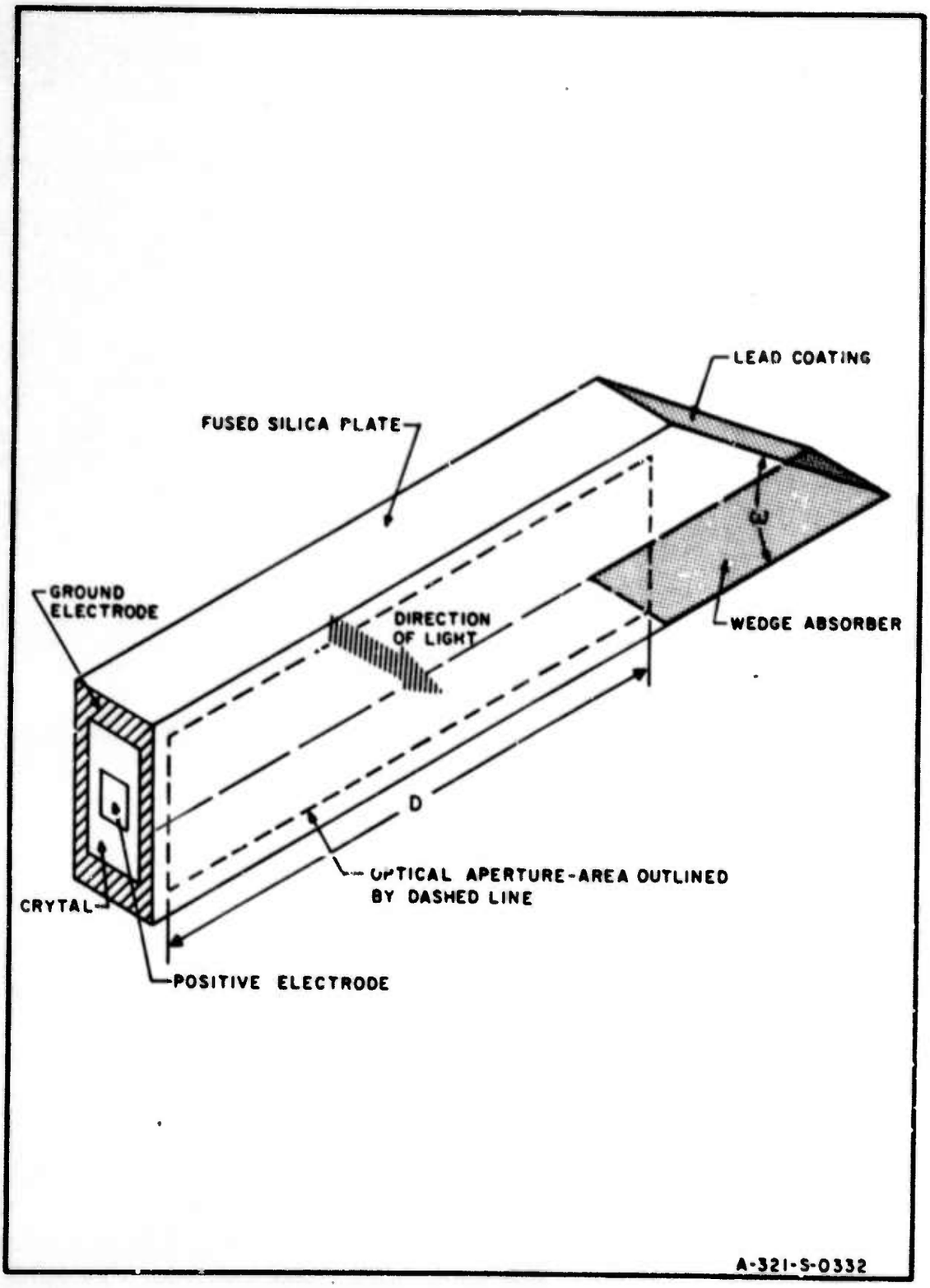

FIG. 8 SINGLE TRANSDUCER SOLID LIGHT MODULATOR CONFIGURATION

edge. If n is odd, the reflected beam will emerge parallel to the incident beam. Thus, greater overall attenuation is possible if n is made an even number.

From experimental tests, the attenuation of the acoustical beam per reflection is on the order of 10 dB, at a fused-silica lead interface. Hence, to obtain 40 dB attenuation 4 reflections are required. A suitable wedge angle is then 36 deg.

The delay medium, itself, is plate or bar shaped depending upon the size of the optical aperture. The faces normal to the optical axis are ground flat and parallel to a degree specified by the application.* The fused-silica material from which the delay line is made is of Schlieren quality so that inhomogeneities and residual strains are kept to a minimum. These, if present to a large degree, can adversely affect the diffraction pattern.

The size of the optical aperture is governed by two factors, the resolution requirements of the system and ultrasonic diffraction. The former controls the integration time T of the modulator where,

$$T = \frac{D}{v_e} , \tag{73}$$

D being the dimension of the aperture in the direction of elastic wave propagation. The integration time can be shown to be inversely proportional to the peak-to-first-null width in the diffraction pattern and, hence, to the resolution of the electro-optical system.[12]

* At this laboratory the severest specifications have been $1/20\lambda$ flatness over any two inch square area, and face parallelism to less than one minute of arc. These specifications have proved adequate for the processor application.

Ultrasonic diffraction causes the elastic beam to spread appreciably beyond the Fresnel region. In this circumstance, the resulting optical diffraction pattern cannot be explained by the plane wave analysis presented here. If the minimum width of the optical aperture, and thus, the width of the transducer, is made large enough, however, the Fresnel region can be extended beyond the aperture length and the undesirable condition eliminated. Therefore, the minimum width of the optical aperture, in the simple light modulator of Fig. 8, is determined by the requirement for maintaining a Fresnel diffraction field throughout the length of the aperture.*

A more complex modulator configuration, applicable to real-time processing of signals received by a radar using a planar array antenna, is shown in Fig. 9. This modulator is capable of simultaneous time and spatial multiplex modes of operation.[12] The number of transducers in the transducer array is governed by the size of the antenna, and constrained by the ultrasonic diffraction effects and practical limitations of the optical system. The multiple absorbing wedges are employed to obtain a maximum optical aperture in a given size plate.

In order to maintain proper electrical phasing in the transducer array (an important requirement in the radar processor application), a common crystal serves all the transducers. This can impose extremely severe conditions on the fabrication of the array, especially at very high frequencies where the crystal will be very thin ($< 30\mu$), but quite long ($\approx$ 3 in.).

* It is assumed that adequate light intensity is available for all aperture widths so that the diffraction pattern is detectable within the system constraints.

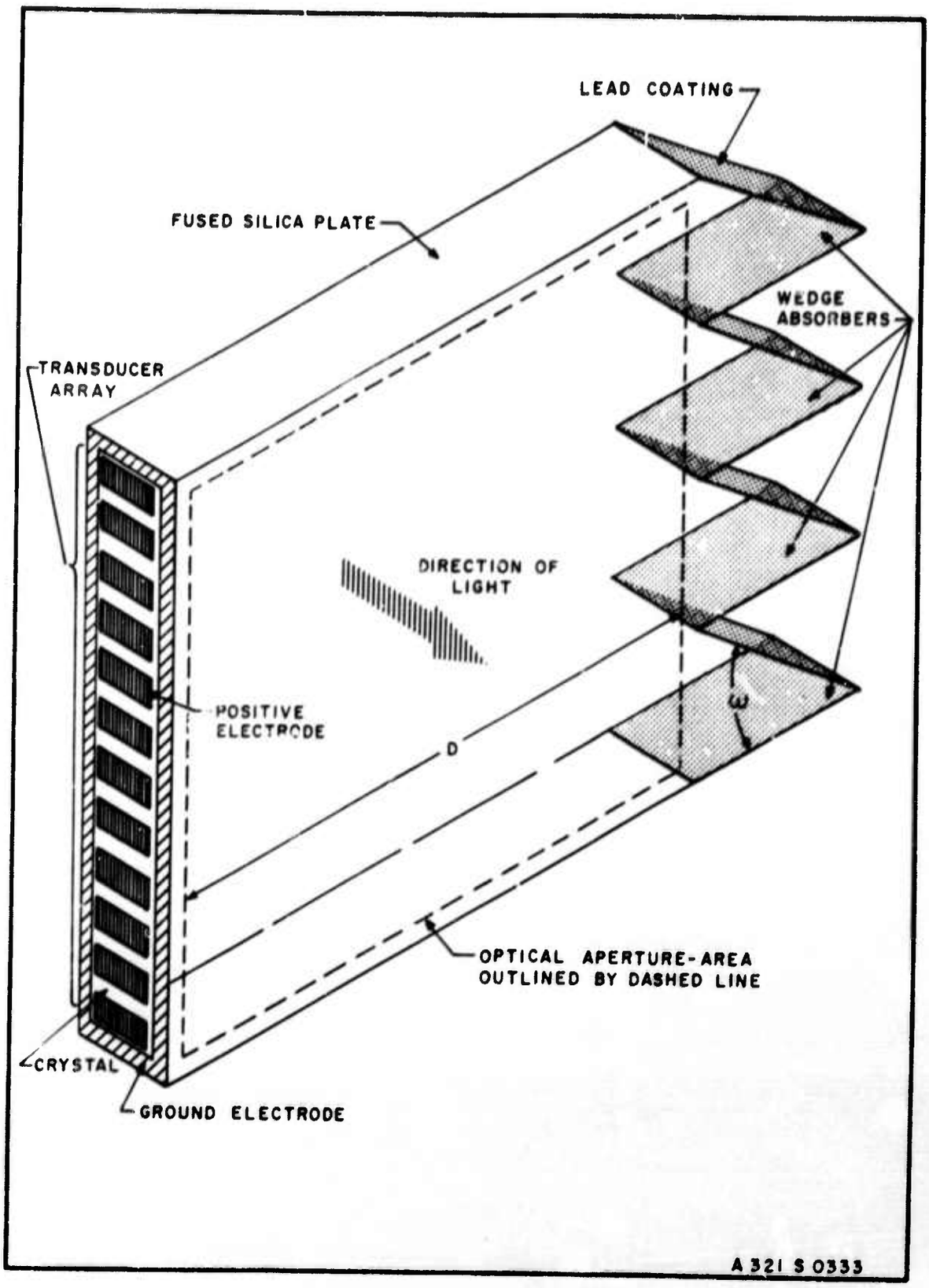

FIG. 9 MULTI-TRANSDUCER SOLID LIGHT MODULATOR CONFIGURATION

In both the simple and the more complex modulator configurations, the minimum thickness of the delay line will be a function of the desired modulation index, the available driver voltage and the optical specifications for the plate. Precision grinding requires that the plate have strong flexural resistance. Hence, even though the strength of the elasto-optic interaction may indicate that a rather thin plate would be satisfactory, the fabrication requirements may actually dictate the allowable minimum thickness.

B. TRANSDUCER CONSIDERATIONS

Quartz transducers, driven at their fundamental frequency, will be used to generate the elastic waves in the solid light modulators under discussion. By choosing the proper crystal cut, either compressional or shear waves will be produced. The X-cut crystal is most suitable for the generation of compressional waves, while a Y-or AC-cut may be used to generate shear waves. In the latter case, however, the AC-cut has been found impractical because the thinness of the crystal at 100 MHz frequency makes it extremely difficult to handle. The treatment to follow, therefore, will be concerned with X- and Y-cut transducers only.

1. General Considerations

The resonant frequency of an X- or Y-cut crystal is inversely proportional to the thickness of the crystal, according to the formula,

$$f_o = \frac{v_c}{2t_c} ,$$

where v_c is the velocity of propagation of the elastic wave in the crystal. Given the resonant frequency in MHz, $\overline{f_o}$, the required thicknesses for each type crystal may be calculated from the relations:

$$t_c = \frac{2.85 \times 10^3}{\overline{f_o}} \qquad \text{X-cut}$$

$$= \frac{1.92 \times 10^3}{\overline{f_o}} \qquad \text{Y-cut}$$

with t_c expressed in microns (μ). Thus, for $\overline{f_o}$ = 100 MHz, the X-cut crystal will have a thickness of 28.5μ and the Y-cut, 19.2μ.

The crystals are attached to the fused-silica delay line by a metallic bond of either lead or indium. This bond can significantly influence the transducer performance, as will be shown. Where a 50 per cent mechanical bandwidth is required, the free crystal face may be left unloaded. For bandwidths on the order of 100 per cent, however, loading is required, with a consequent reduction in force at the transducer-delay line interface.

The electromechanical equivalent circuit for an air-backed X-or Y-cut transducer, including the bond, which is assumed lossless, is shown in Fig. 10.[18] The crystal parameters are the static capacitance C_o, the electromechanical transformer ratio Φ, and the mechanical impedance of the crystal Z_c. The bond parameters are the mechanical impedance of the bond material Z_b, and the wavelength thickness of the bond, δ. The element Z_q repre-

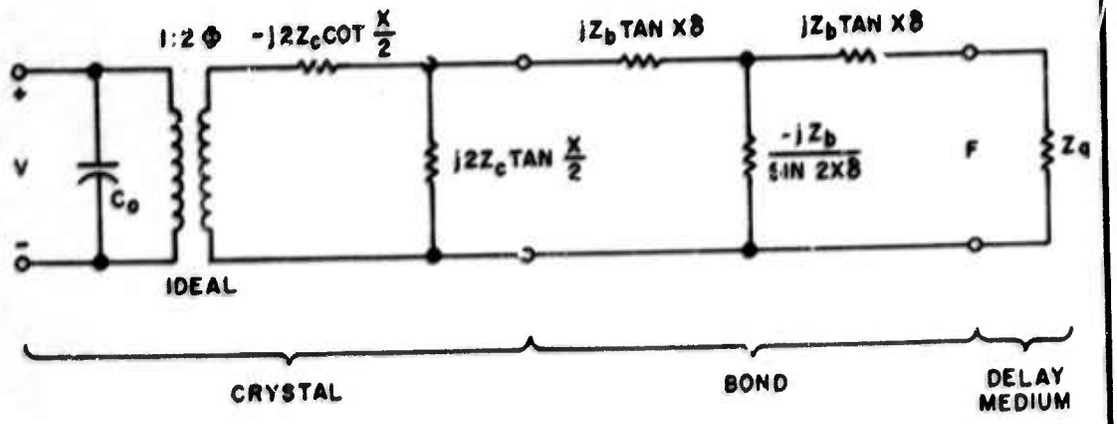

C_o = STATIC CAPACITANCE OF CRYSTAL
Φ = ELECTROMECHANICAL TRANSFORMER RATIO
Z_c = MECHANICAL IMPEDANCE OF CRYSTAL
Z_b = MECHANICAL IMPEDANCE OF BOND
Z_q = MECHANICAL IMPEDANCE OF DELAY MEDIUM
V = APPLIED VOLTAGE
F = FORCE AT TRANSDUCER-MEDIUM INTERFACE
$X = \pi f / f_o$
$\delta = t_b / \lambda_b$

A-321-S-0260

FIG. 10 ELECTROMECHANICAL EQUIVALENT CIRCUIT FOR X AND Y-CUT QUARTZ TRANSDUCERS INCLUDING THIN ADHESIVE BOND

sents the mechanical impedance of the fused-silica delay medium, which is real, and the parameter x is frequency dependent and defined as

$$x \equiv \pi \frac{f}{f_o}$$

where f is the electrical excitation frequency in Hz.

In quantitative terms, the crystal parameters, as functions of the resonant frequency and the effective transducer area A in m^2, are:[20]

$C_o = 1.425 \times 10^4 \overline{f_o} A$	pf	X-cut
$= 2.11 \times 10^4 \overline{f_o} A$	pf	Y-cut
$\Phi = 60.6 \overline{f_o} A$	coulombs/m	X-cut
$= 89.2 \overline{f_o} A$	coulombs/m	Y-cut
$Z_c = 15.1 \times 10^6 A$	kg/sec	X-cut
$= 10.1 \times 10^6 A$	kg/sec	Y-cut

The mechanical impedance of the bond and the delay medium depends upon the type of wave being propagated as well as the choice of material. When compressional waves are excited,

$$Z_q = 13.1 \times 10^6 A \quad \text{kg/sec}$$

and, according to a relatively recent source,[21]

$$Z_b = 24.6 \times 10^6 A \quad \text{kg/sec}$$

for a thin lead bond, and

$$Z_b = 18.3 \times 10^6 A \qquad \text{kg/sec}$$

for a thin indium bond. The corresponding shear wave case is covered by the expressions:

$$Z_q = 8.29 \times 10^6 A \qquad \text{kg/sec}$$

$$Z_b = 8.0 \times 10^6 A \qquad \text{kg/sec} \qquad \text{(lead)}$$

$$Z_b = 5.2 \times 10^6 A \qquad \text{kg/sec} \qquad \text{(indium)}$$

where Z_b (indium) differs from the expression given in the source cited because it appears to be incorrect there, on the basis of data received by CUERL.[19]

The wavelength thickness of the bond, δ, is a dimensionless parameter defined by

$$\delta = \frac{t_b}{\lambda_b}$$

where t_b is the actual bond thickness and λ_b is the wavelength of the excited wave in the bond.

The values of the frequency dependent parameters are given in Table I for the two frequencies of interest, 80 and 100 MHz. Determination of the required effective area depends upon other considerations which will be discussed subsequently.

TABLE I

X- & Y-CUT TRANSDUCER PARAMETER VALUES AT 80 AND 100 MHz

PARAMETER	X-Cut (Compressional)		Y-Cut (Shear)	
	80 MHz	100 MHz	80 MHz	100 MHz
t_c Microns	35.6	28.5	24.0	19.2
C_o/A $\frac{Pf}{M^2}$	114×10^4	142×10^4	168.8×10^4	211×10^4
Φ/A $\frac{Coulombs}{M^3}$	4848	6060	7136	8920

t_c = thickness of transducer crystal

C_o = static capacitance of crystal

Φ = electromechanical transformer ratio

A = effective transducer area

2. Transducer Performance with Zero-Thickness Bond

When the bond thickness is zero, $\delta = 0$ and the bond elements in the equivalent circuit of Fig. 10 have no effect upon the transducer performance. This is the so-called "ideal" case which is most important in determining the nominal characteristics of the transducer in the preliminary design of the solid light modulator.

The force F at the transducer-delay medium interface, in this circumstance, is given by

$$\left| \frac{F}{F_o} \right| = \frac{1}{(1 - \cot^2 \frac{x}{2})(1 + c^2 \tan^2 x)^{\frac{1}{2}}} \tag{74}$$

where

$$F_o = 2\Phi V , \tag{75}$$

the generated force at $f = f_o$ (i.e., at the crystal resonant frequency), and

$$c \equiv \frac{Z_c}{Z_q} .$$

From Eq. (74), the frequency response of an X- and Y-cut transducer radiating into a semi-infinite fused-silica delay medium can be determined. Figure 11 shows these responses as a function of the normalized frequency f/f_o. Note that, in both cases, 50 per cent bandwidths are easily achieved without the aid of backing. And, for all practical purposes, the attainable unbacked transducer bandwidth is the same for both transducers.

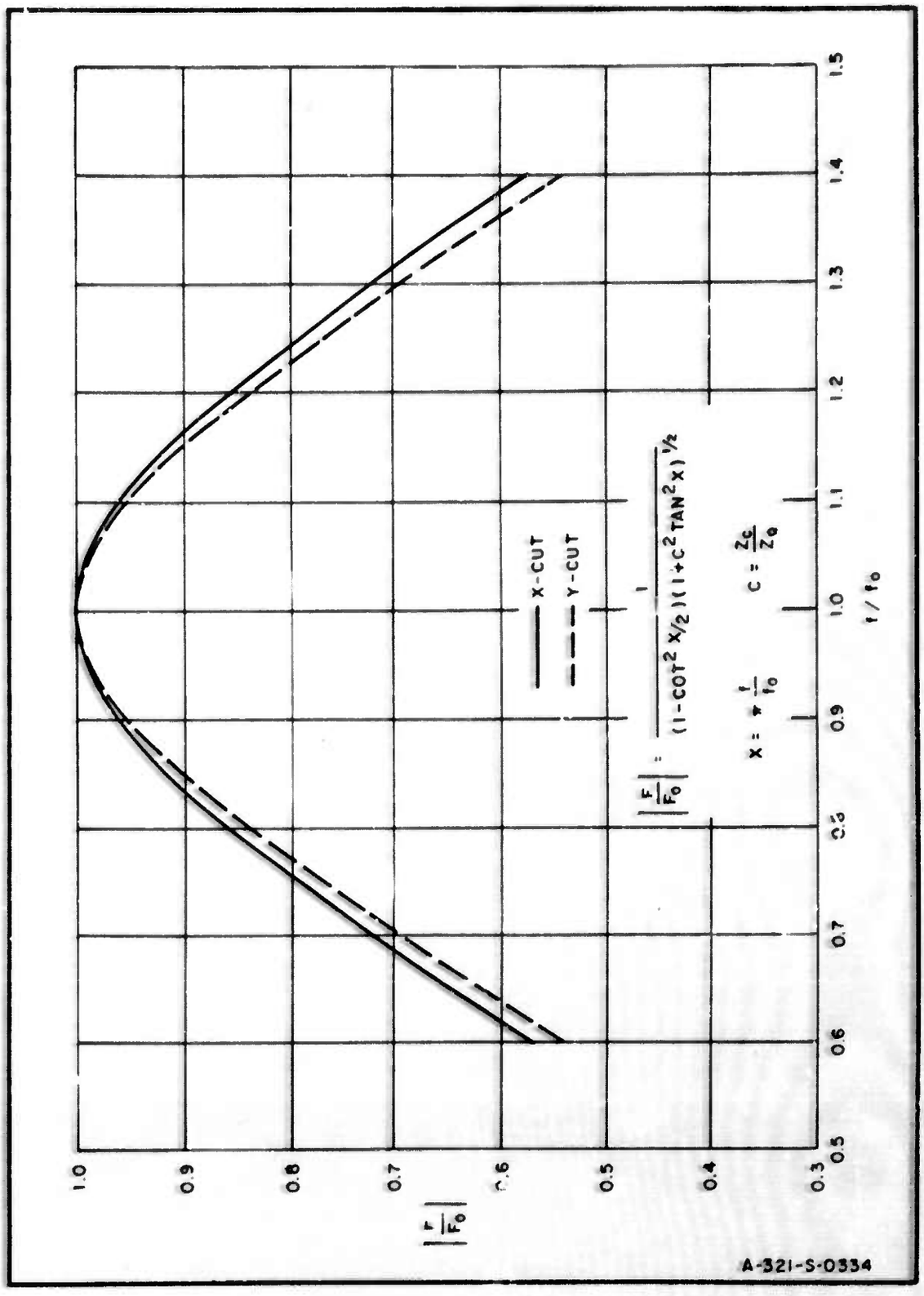

FIG. 11 IDEAL FREQUENCY RESPONSE OF SINGLE, AIR-BACKED TRANSDUCERS RADIATING INTO NON-REFLECTIVE FUSED-SILICA MEDIUM

The input impedance, at resonance, is an important parameter because it determines the load characteristics for the transducer driver. Referring to the equivalent circuit, it is seen that when $f \approx f_o$, the only load on the electromechanical transformer is Z_q. Hence, the electrical load presented to the driver is a simple parallel RC network whose parameter values are (neglecting external factors):

$$R_i = \frac{Z_q}{4\Phi^2} \quad \text{ohms}$$

$$C_i = C_o \quad \text{pf}$$

when Z_q is in kg/sec and Φ is in coulombs/m.

The average power absorbed by the transducer is given by

$$P_{av} = \frac{F_m^2}{2Z_q} ,$$

when the excitation is sinusoidal and generates a force amplitude F_m. At the resonant frequency,

$$F_m = 2\Phi V_m$$

by Eq. (75), and thus,

$$P_{av} = \frac{2\Phi^2 V_m^2}{Z_q} .$$

Since both ϕ and Z_q are functions of the area A, the parametric dependence of the average absorbed power may be expressed more specifically as,

$$P_{av} = 561A\bar{f}_o^2 v_m^2 \times 10^{-6} \qquad \text{X-cut}$$

$$= 1917A\bar{f}_o^2 v_m^2 \times 10^{-6} \qquad \text{Y-cut}$$

where P_{av} is in watts.

The working forms of the equations for determining P_{av}, R_i and C_i at 80 and 100 MHz are given in Table II.

3. Transducer Performance with Non-Zero Thickness Bond

When the bond thickness is not zero, but some fraction of a wavelength, the normalized force at the interface may be expressed in the form,

$$\left|\frac{F}{F_o}\right| = \left\{\left[(1 - \cot^2\tfrac{x}{2})\cos 2x\delta + (\tfrac{2c}{b})\cot\tfrac{x}{2}\sin 2x\delta\right]^2 + b^2\left[(\tfrac{2c}{b})\cot\tfrac{x}{2}\cos 2x\delta - (1 - \cot^2\tfrac{x}{2})\sin 2x\delta\right]^2\right\}^{-1}, \tag{76}$$

where

$$b \equiv \frac{Z_b}{Z_q}$$

is the normalized bond impedance.

At the crystal resonant frequency, $f = f_o$, the parameter $x = \pi$, and Eq. (76) reduces to

TABLE II

X-& Y-CUT TRANSDUCER ELECTRICAL PARAMETER FORMULAS AT RESONANT FREQUENCIES OF 80 AND 100 MHz - ZERO-THICKNESS BOND

PARAMETER	X-Cut (Compressional)		Y-Cut (Shear)	
	80 MHz	100 MHz	80 MHz	100 MHz
R_i ohms	$\frac{0.139}{A}$	$\frac{0.089}{A}$	$\frac{0.041}{A}$	$\frac{0.026}{A}$
$C_i = C_o$ pf	$114A \times 10^4$	$142.5A \times 10^4$	$169A \times 10^4$	$211A \times 10^4$
P_{av} watts	$3.59AV_m^2$	$5.61AV_m^2$	$12.27AV_m^2$	$19.17AV_m^2$

R_i = input resistance of transducer

C_i = input capacitance of transducer

P_{av} = average absorbed power

A = effective transducer area in m^2

V_m = applied voltage amplitude

$$\left| \frac{F}{F_o} \right|_{f = f_o} = (\cos^2 2\pi\delta + b^2 \sin^2 2\pi\delta)^{-1} .$$

This normalized force is plotted in Fig. 12 as a function of δ, for X-and Y-cut crystals bonded with lead and indium to the fused-silica delay medium. It should be noted that the difference in the shapes of the curves is solely dependent upon the normalized bond impedance b.

The LEAD-SHEAR curve exhibits the least change in $|F|F_o|$ with δ. This is indicative of the fact that the mechanical impedance of the lead closely matches that of the fused-silica in shear operation. The value of b in this case is 0.965.

As the impedance mismatch increases, the variation of $|F|F_o|$ with changes in δ increases. When a lead bond is used with an X-cut crystal, $b = 1.88$, and rapid variation occurs, reaching a minimum of $F \simeq 0.5\ F_o$ at $\delta = 0.25$ and 0.75. With an indium bond, however, the variation is significantly smaller since $b = 1.4$. It appears, then, on the basis of these curves, that it is advantageous to bond an X-cut crystal with indium rather than lead in order to decrease the bond thickness sensitivity of the transducer. In both cases, as will be shown, a wavelength bond thickness less than $\delta = 0.025$ will be necessary if maximum response and bandwidth are to be achieved.

The INDIUM-SHEAR curve shows the sharpest variation in response with changes in δ, but in the opposite direction. This is characteristic of bonds whose b values are less than one (here $b = 0.627$). Outside of the dif-

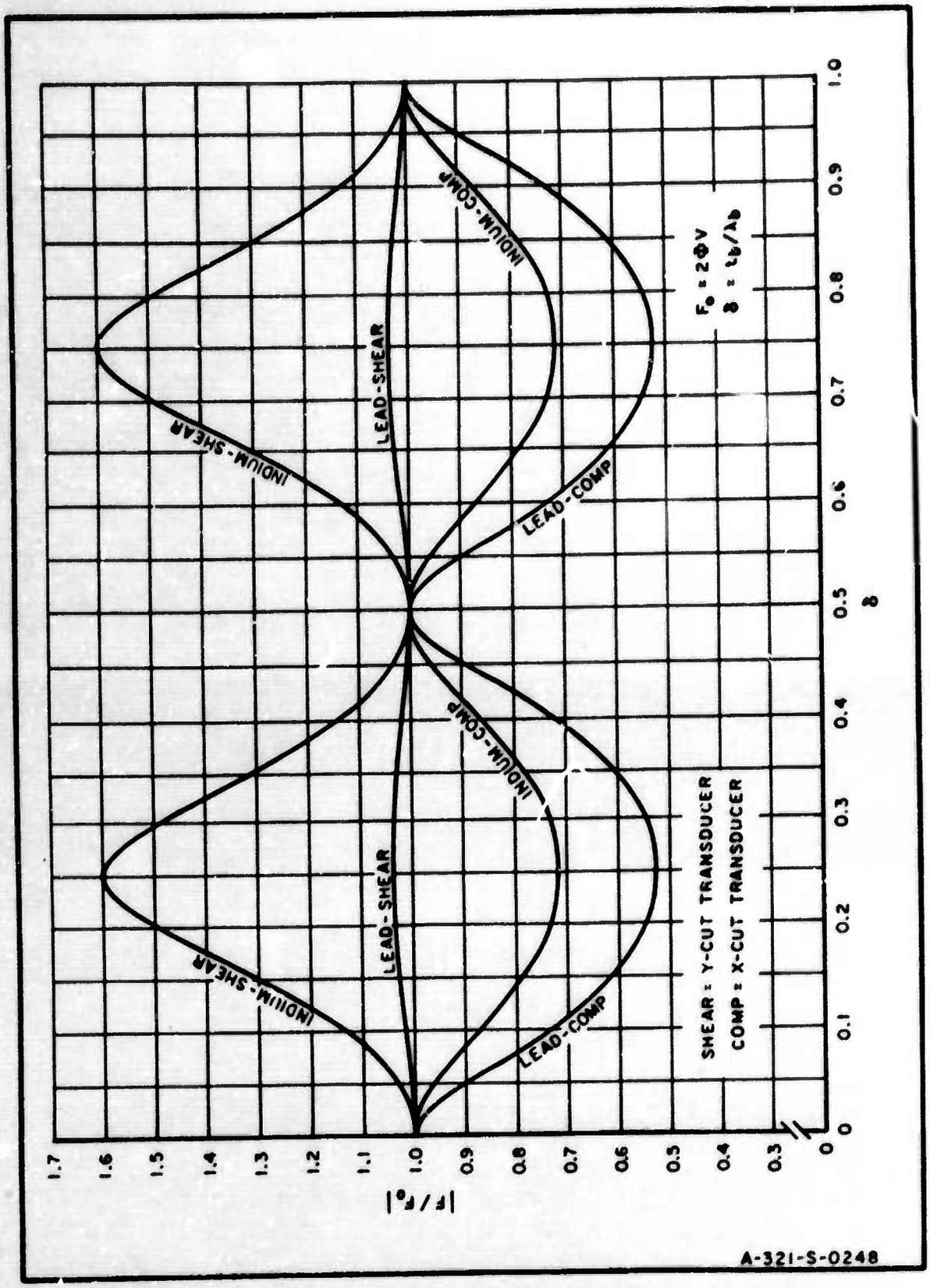

FIG. 12 TRANSDUCER MECHANICAL RESPONSE AT CRYSTAL RESONANT FREQUENCY vs. BOND WAVELENGTH THICKNESS FOR LEAD AND INDIUM BONDS

ficulty of bonding with lead, there is no apparent reason for choosing indium as the bonding material with Y-cut transducers, since the lead bond so obviously displays an almost ideal character. If indium is used, however, maximum performance will only be achieved if δ is again less than 0.025.

Although all the curves in Fig. 12 are symmetrical about $\delta = 0.5$, it cannot be assumed that the frequency response will also be symmetrical about this value. Quite the contrary turns out to be the case, as shown below, so that any attempt to obtain optimal transducer performance must be made in the direction of minimum thickness bonds.

The frequency response of the transducers under consideration can now be obtained from Eq. (76), by letting x vary over the range $\frac{\pi}{2} \leq x \leq \frac{3\pi}{2}$ for selected values of δ. The response curves are plotted in Figs. 13 - 16.

Fig. 13a shows the variations in response for an X-cut crystal bonded to the fused-silica delay medium with lead of thicknesses $\delta = 0.01$, 0.05 and 0.1. The $\delta = 0$ curve is also plotted to establish a reference. The high sensitivity to bond thickness is clearly evident along with the rapid shift in peak response toward lower frequencies as δ increases. Reduced bandwidth and increased asymmetry accompanies the shift.

The formation of double- and triple-peaked response, first beginning to appear in the $\delta = 0.1$ curve, is shown clearly in Fig. 13b, where the $\delta = 0.25$, 0.5, 0.75 and 1.0 curves are plotted. The $\delta = 0.5$ curve is essentially single-peaked but its bandwidth is significantly less than the curves for $\delta < 0.25$. Thus, its possible use in the light modulators of concern to this project is eliminated.

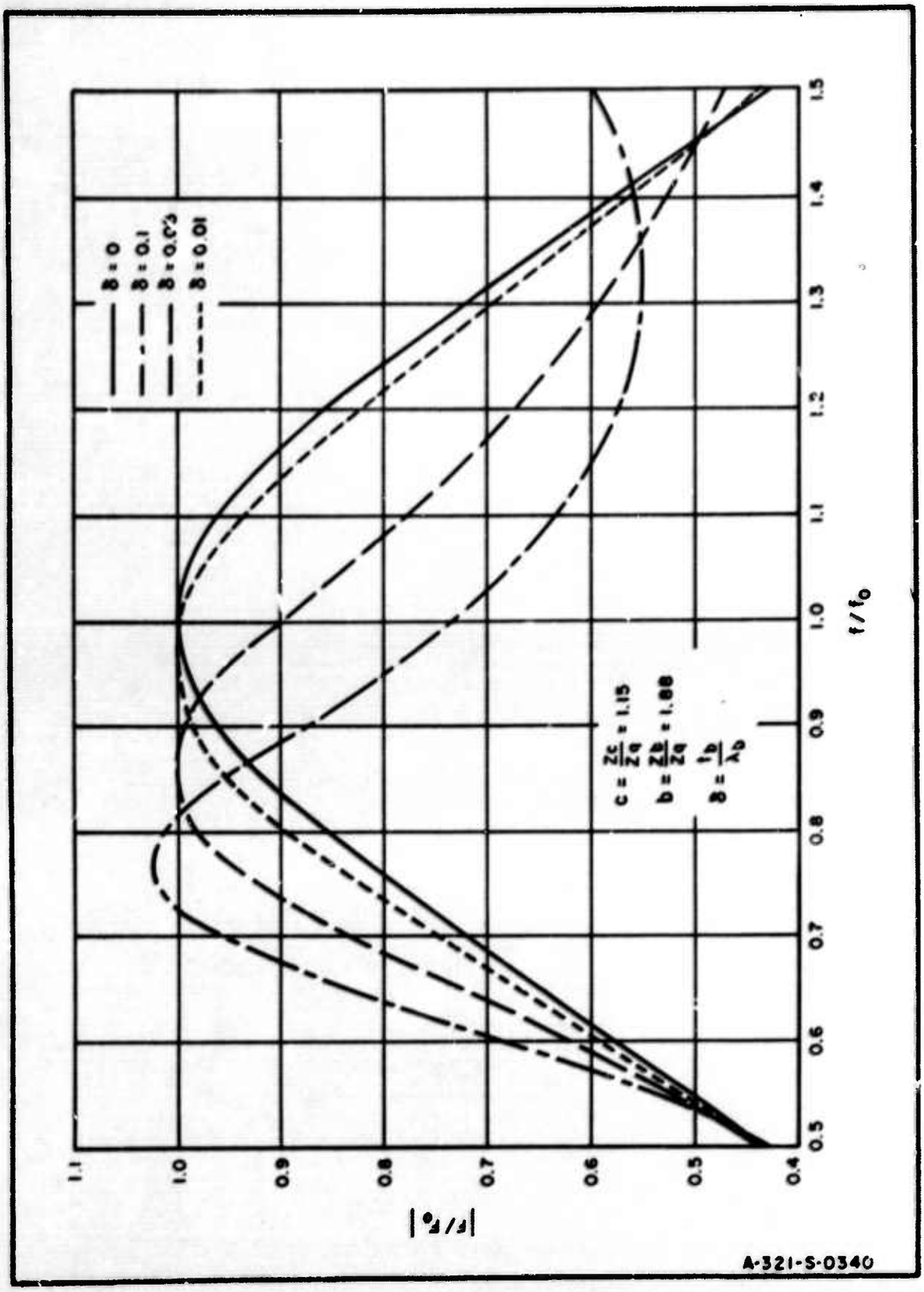

FIG. 13a MECHANICAL RESPONSE OF X-CUT TRANSDUCER WITH LEAD BOND TO FUSED-SILICA DELAY MEDIUM

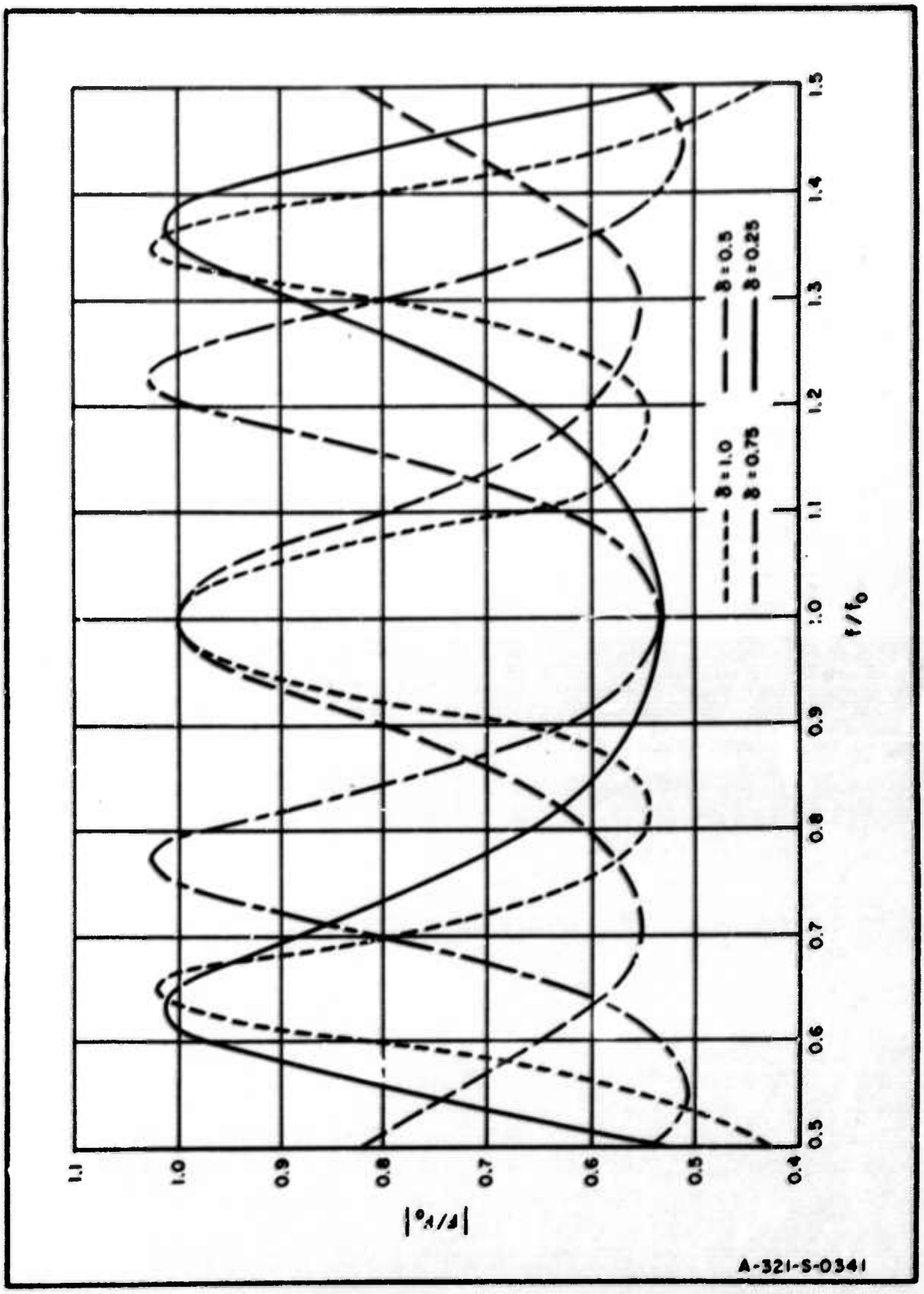

FIG. 13b MECHANICAL RESPONSE OF X-CUT TRANSDUCER WITH LEAD BOND TO FUSED-SILICA DELAY MEDIUM

If operation of the X-cut transducer with lead bond requires full 50 per cent bandwidth, centered very close to the crystal resonant frequency, it is necessary, according to Fig. 13a, that the bond thickness be much less than $\delta = 0.05$.

As a measure of the actual thicknesses involved, calculations of bond thicknesses in microns, at 80- and 100-MHz frequencies, have been made and are presented in Table III for the values of δ appearing in the response curves. It can now be noted that at 100 MHz, t_b is only 1.1μ when $\delta = 0.05$ with lead.

The mechanical response of a Y-cut crystal with lead bond is shown in Figs. 14a and b. The good mechanical match between the bond and the medium maintains almost symmetrical response about $f = f_o$, regardless of the value of δ. Bandwidth is also preserved in all cases. Hence, the bond thickness has negligible effect upon the performance of this transducer. This offers a distinct advantage when spatially multiplexed modulators, which require large common crystals uniformly bonded to the delay medium, are under consideration.

Improved compressional wave transducer response is possible when indium is substituted for lead in the bond. This is clearly indicated in Figs. 15a and b, and reinforces the prediction of this result made on the basis of the curves in Fig. 12. Indium is easier to bond with and, for a given δ, has a slightly greater thickness (Table III).

Figures 16a and b show the response to be expected from an indium-bonded Y-cut crystal. Because $b < 1$, the curves for small δ tend to have peak responses at frequen-

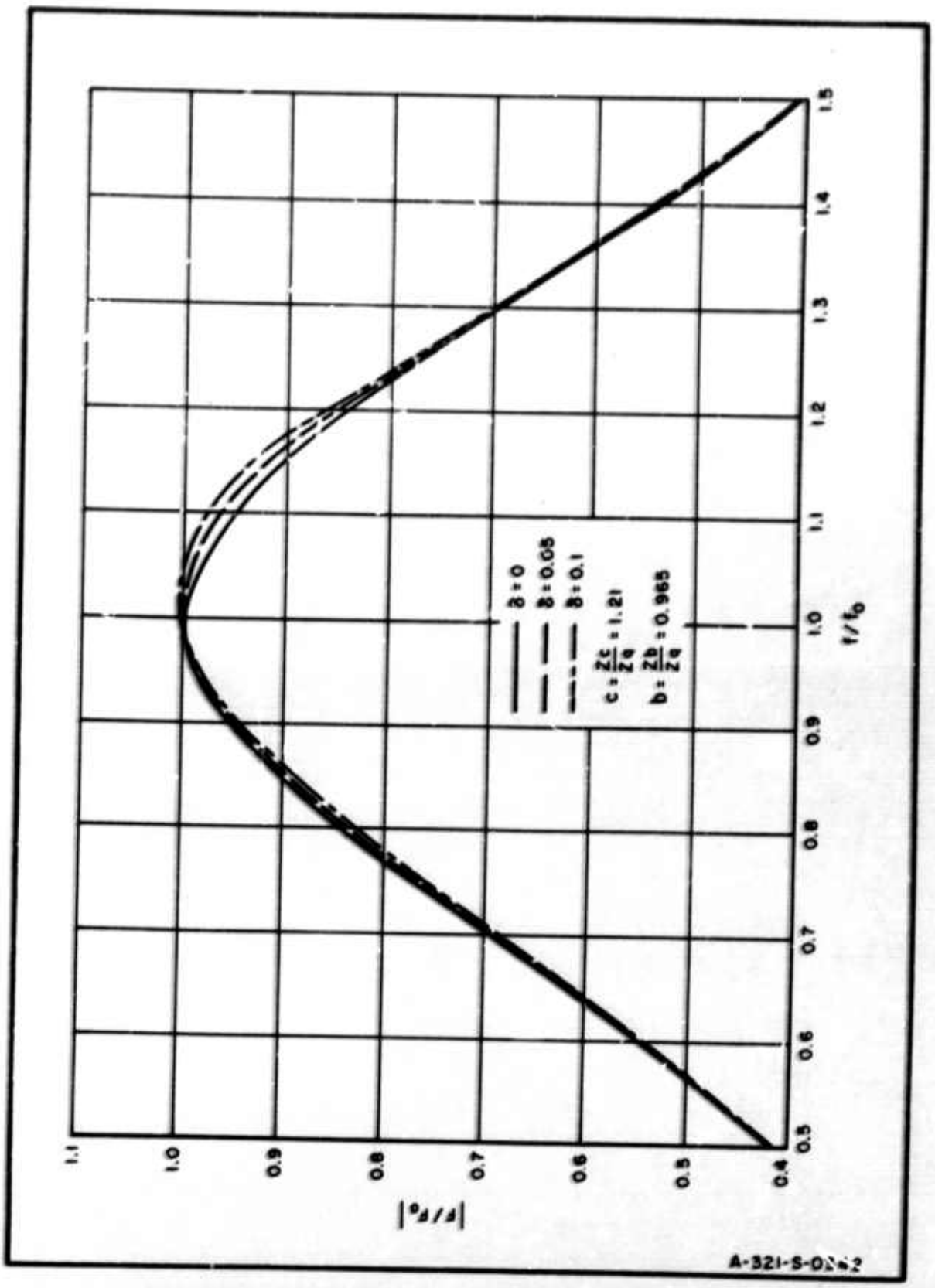

FIG. 14a MECHANICAL RESPONSE OF Y-CUT TRANSDUCER WITH LEAD BOND TO FUSED-SILICA DELAY MEDIUM

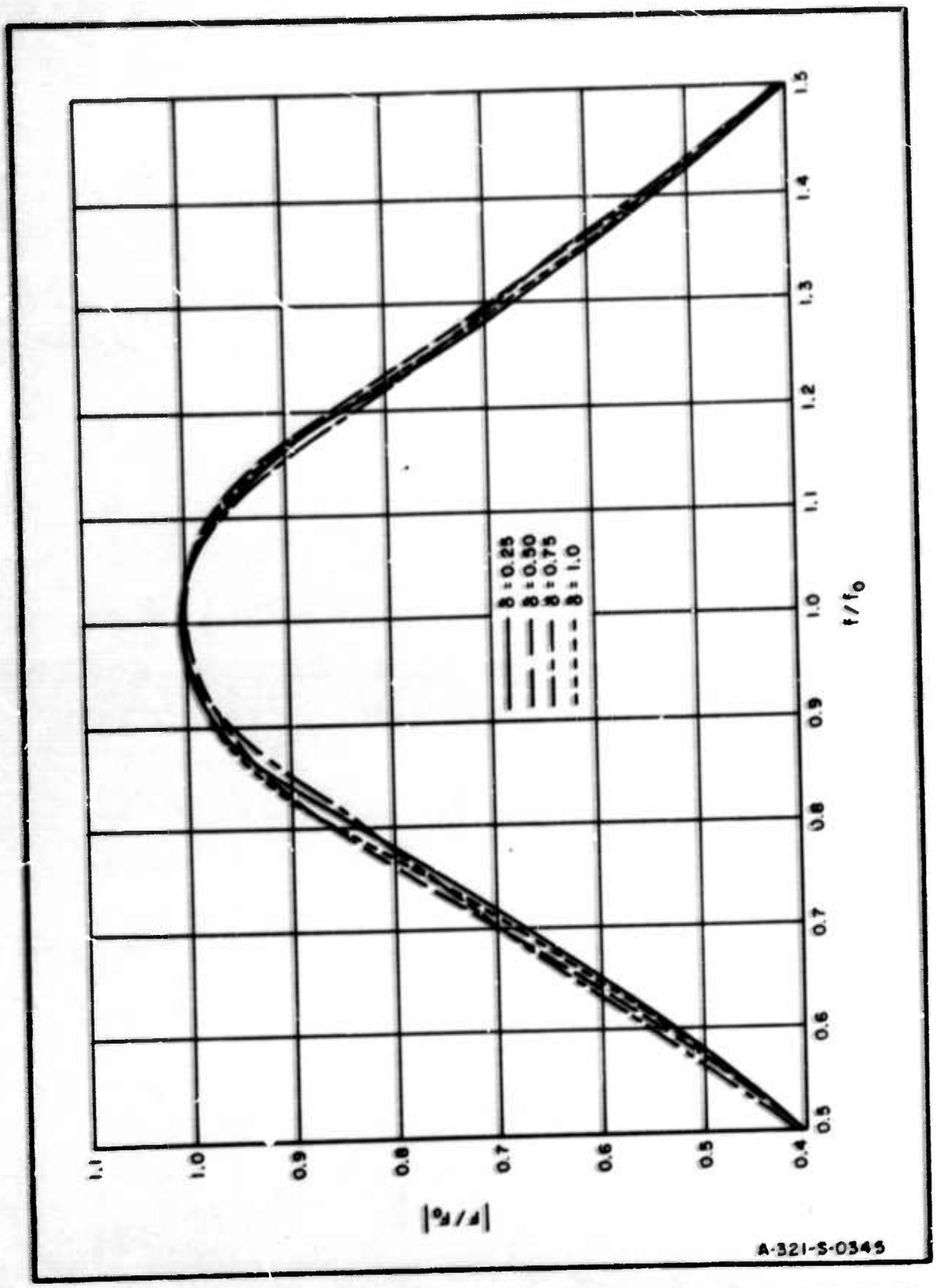

FIG. 14b MECHANICAL RESPONSE OF Y-CUT TRANSDUCER WITH LEAD BOND TO FUSED-SILICA DELAY MEDIUM

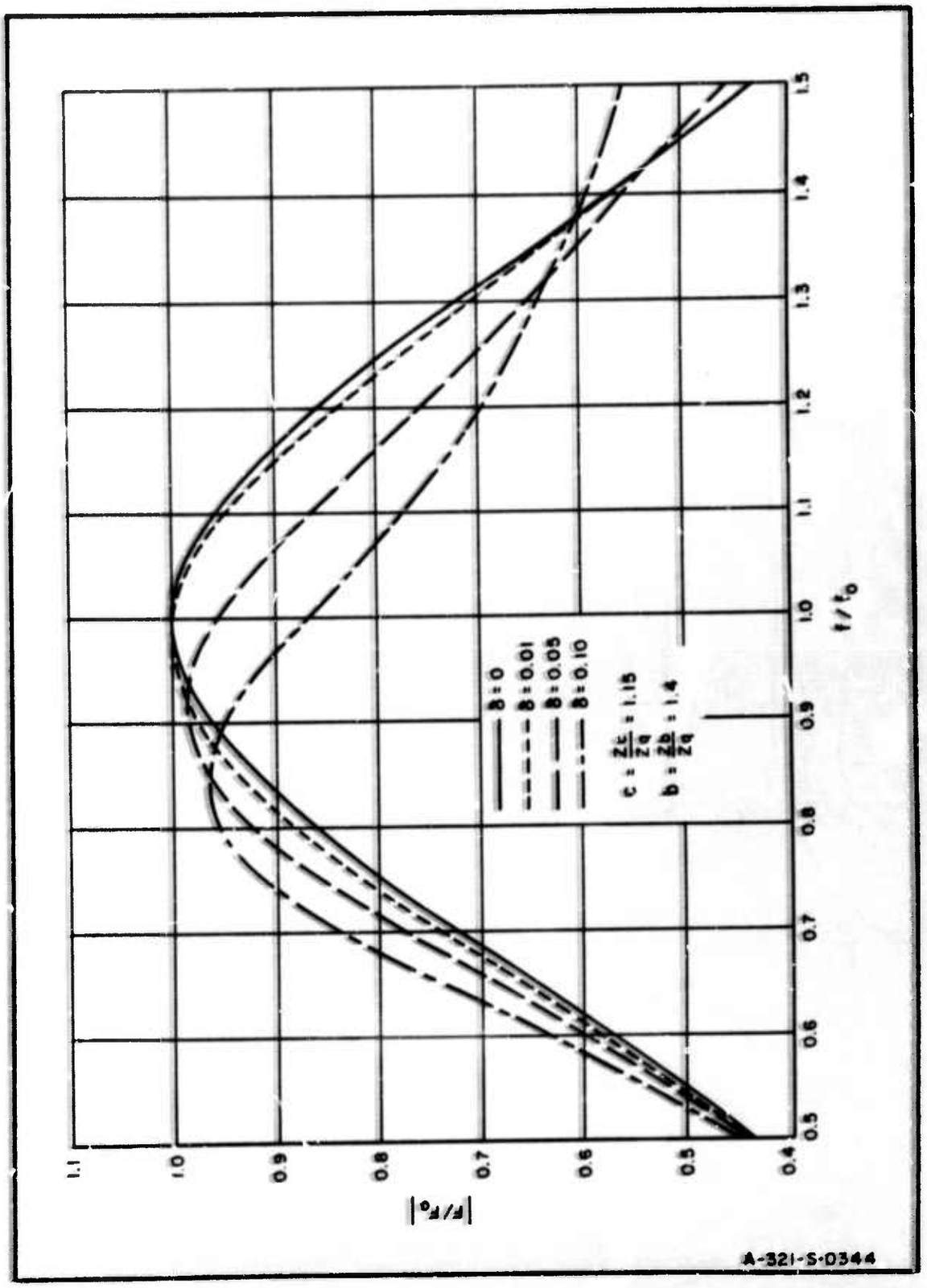

FIG. 15a MECHANICAL RESPONSE OF X-CUT TRANSDUCER WITH INDIUM BOND TO FUSED-SILICA DELAY MEDIUM

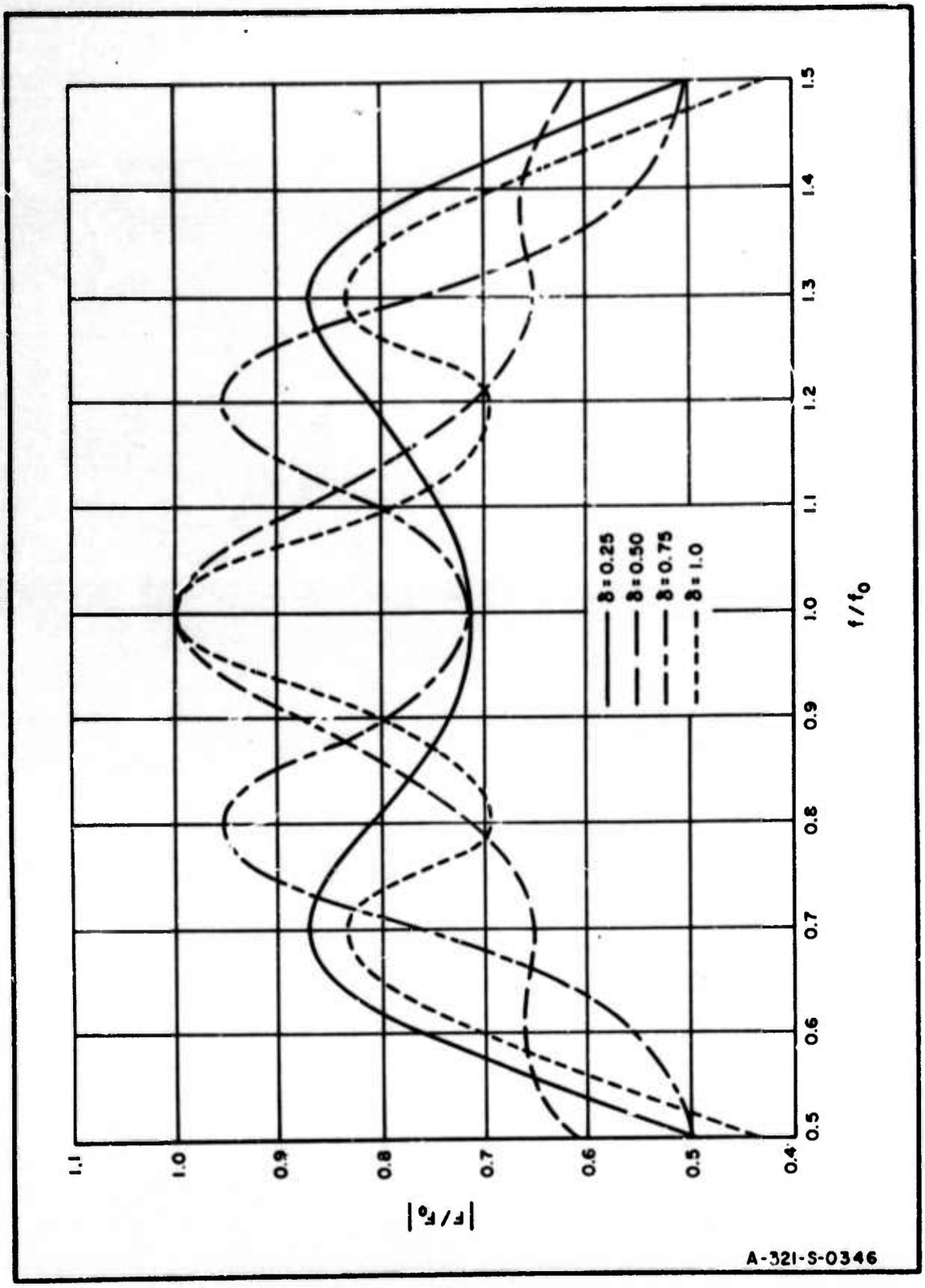

FIG. 15b MECHANICAL RESPONSE OF X-CUT TRANSDUCER WITH INDIUM BOND TO FUSED-SILICA DELAY MEDIUM

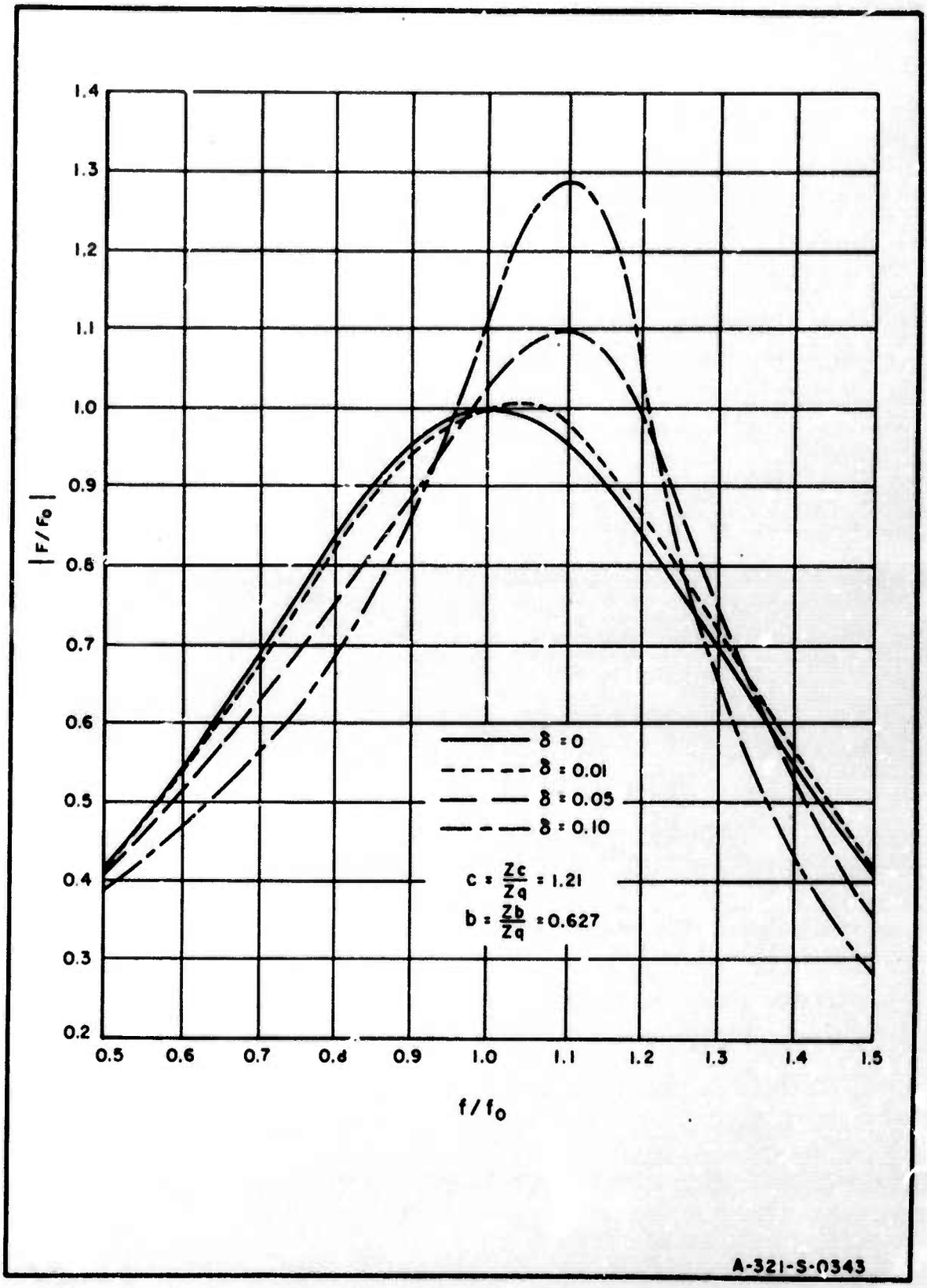

FIG. 16a MECHANICAL RESPONSE OF Y-CUT TRANSDUCER WITH INDIUM BOND TO FUSED-SILICA DELAY MEDIUM

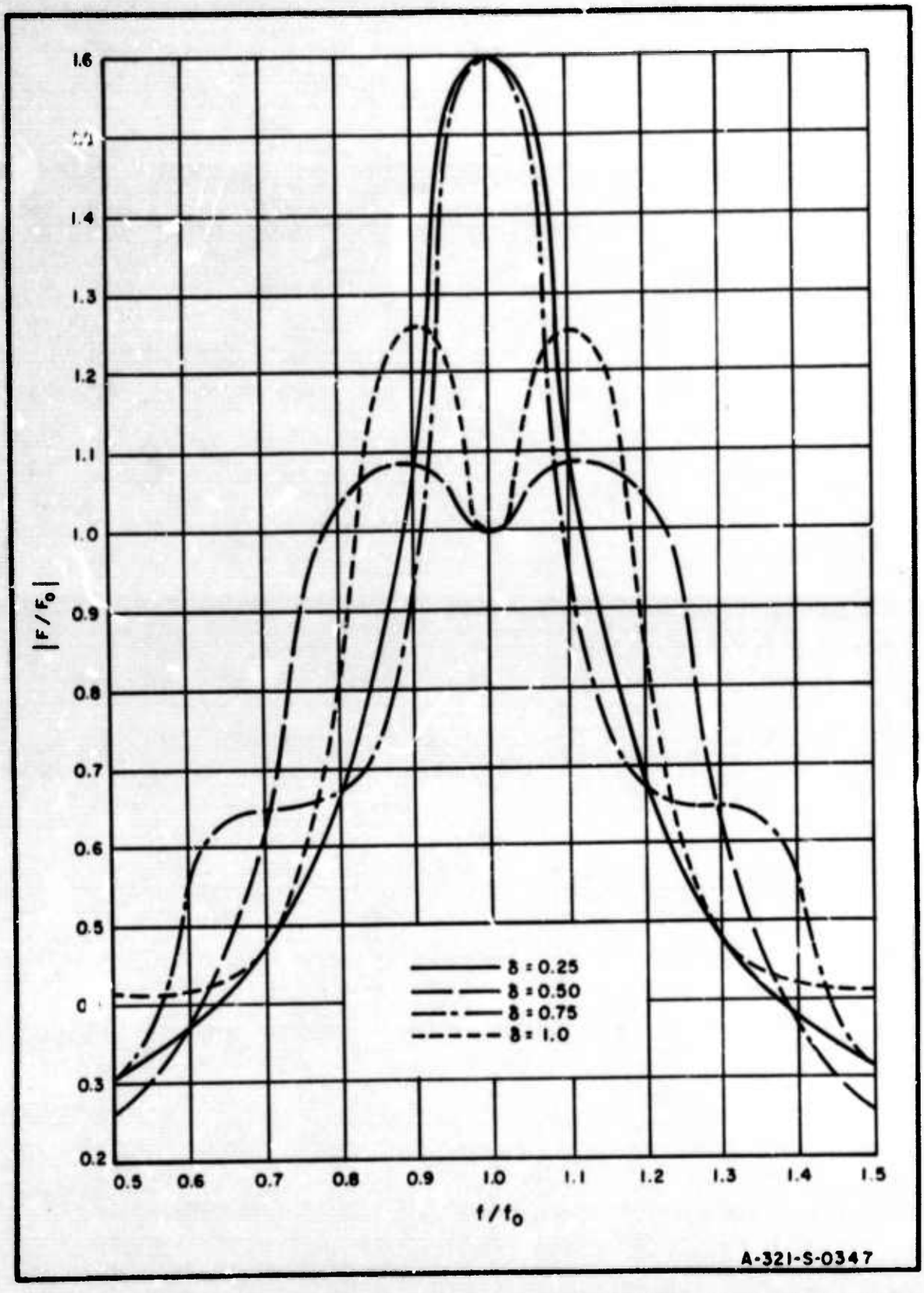

F.G. 16b MECHANICAL RESPONSE OF Y-CUT TRANSDUCER WITH INDIUM BOND TO FUSED-SILICA DELAY MEDIUM

TABLE III

BOND THICKNESS IN MICRONS VS δ FOR LEAD & INDIUM

$1\mu = 10^{-6}$ M

LEAD BOND

δ	Compressional Wave		Shear Wave	
	80 MHz	100 MHz	80 MHz	100 MHz
0.01	0.27	0.22	0.089	0.071
0.05	1.35	1.10	0.445	0.355
0.1	2.70	2.20	0.890	0.710
0.25	6.75	5.50	2.225	1.775
0.5	13.50	11.00	4.450	3.550
0.75	20.25	16.50	6.675	5.325
1.0	27.00	22.00	8.900	7.100

INDIUM BOND

δ	Compressional Wave		Shear Wave	
	80 MHz	100 MHz	80 MHz	100 MHz
0.01	0.31	0.25	0.089	0.071
0.05	1.55	1.25	0.445	0.355
0.1	3.10	2.50	0.890	0.710
0.25	7.75	6.25	2.225	1.775
0.5	15.50	12.50	4.450	3.550
0.75	23.25	18.75	6.675	5.325
1.0	31.00	25.00	8.900	7.100

cies above f_o. However, when $\delta = 0.25$ and above, the response becomes symmetrical about $f = f_o$, with generally reduced bandwidth. It is of interest to note that at $\delta = 0.25$, F is approximately 60 per cent greater than it would be in the ideal case, $\delta = 0$. This enhancement in the response might be useful in certain narrow-band applications, but is of little concern here. Table III indicates that at 100 MHz, $t_b = 1.775\mu$ when $\delta = 0.25$. Therefore, it is easy to deposit an indium layer of this thickness with present deposition techniques.

C. MODULATION INDEX VS APPLIED VOLTAGE

The relationship between the modulation index and the voltage applied to the transducer can now be established by Eqs. (63), (64) and (75). It is assumed that the excitation is sinusoidal, with amplitude V_m and frequency f_o, and the transducer bond approximates the ideal zero thickness. Then, by Eq. (75),

$$F_m = 2\Phi V_m$$

and the maximum stress T_m is just

$$T_m = \frac{F_m}{A} = 2\left(\frac{\Phi}{A}\right)V_m \tag{77}$$

where it is further assumed that the transducer action is uniform over the effective area A.

Applying Eq. (77) to Eqs. (63) and (64) gives the following relationships for L and T waves, respectively:

$$\psi_{m_{1L}} = \frac{4\pi}{\lambda_L}\left(\frac{1+\sigma}{E}\right)n_o^2 qL\left(\frac{\Phi_x}{A}\right)V_m$$

$$\psi_{m_{2L}} = \frac{4\pi}{\lambda_L}\left(\frac{1+\sigma}{E}\right)n_o^2 pL\left(\frac{\Phi_x}{A}\right)V_m \qquad (78)$$

$$\psi_{m_{1T}} = \psi_{m_{2T}} = \frac{2\pi}{\lambda_L} BL\left(\frac{\Phi_y}{A}\right)V_m \qquad (79)$$

where Φ_x is the electromechanical transformer ratio for the X-cut transducer and Φ_y is that for the Y-cut transducer. All other terms correspond to those defined previously, and, since only magnitudes are of interest here, the signs of the ψ_m have been neglected.

The working forms of these equations, at 80- and 100-MHz resonant frequencies, can be obtained by substitution of the appropriate values for all the quantities on the right except L and V_m, which are independent parameters. The appropriate values are listed in Tables I and IV, where the value for λ_L is taken as that of the He-Ne laser light source being used in the experimental program at CUERL. With these values, Eqs. (78) and (79) reduce to:

$\underline{f_o = 80\ \text{MHz}}$

$$\psi_{m_{1L}} = 27.6 \times 10^{-4} L\, V_m \qquad (80)$$

TABLE IV

VALUES OF CONSTANT PARAMETERS USED IN DERIVATION OF EQS. (80) & (81)

$\lambda_L = 0.633 \times 10^{-6}$ m

$\sigma = 0.164$

$E = 0.76 \times 10^{11}$ newtons/m^2

$n_o = 1.46$

$q = 0.088$

$p = 0.197$

} Measured with 0.589μ light wavelength*

$B = 3.51 \times 10^{-12}$ m^2/newton measured with 0.644μ light wavelength*

*Primak, W., and Post, D., "Photoelastic Constants of Vitreous Silica and Its Elastic Coefficient of Refractive Index," Journal of Applied Physics, Vol. 30, No. 5, May 1959.

f_o = 80 MHz (Cont'd.)

$$\psi_{m_{2L}} = 61.7 \times 10^{-4} L\, V_m$$

$$\psi_{m_{1T}} = \psi_{m_{2T}} = 25 \times 10^{-4} L\, V_m \qquad (80)$$

f_o = 100 MHz

$$\psi_{m_{1L}} = 34.5 \times 10^{-4} L\, V_m$$

$$\psi_{m_{2L}} = 77.2 \times 10^{-4} L\, V_m \qquad (81)$$

$$\psi_{m_{1T}} = \psi_{m_{2T}} = 31.2 \times 10^{-4} L\, V_m$$

where L is in cm for convenience, and V_m is in volts.

As an example of the voltages required to achieve a desired modulation index $\psi_m \leq 0.3$ radian,* the second and third formulas in Eqs. (80) and (81) are plotted in Figs. 17 and 18, for selected values of L, where the direction of polarization of the incident light has been chosen to be in

* Lambert[12] has shown that to maintain a dynamic range of $\geq$ 40 dB, ψ_m must be ≤ 0.3 radian. The dynamic range is defined as the ratio of the peak signal intensity to the peak spurious response intensity in the image plane of the electro-optical processor.

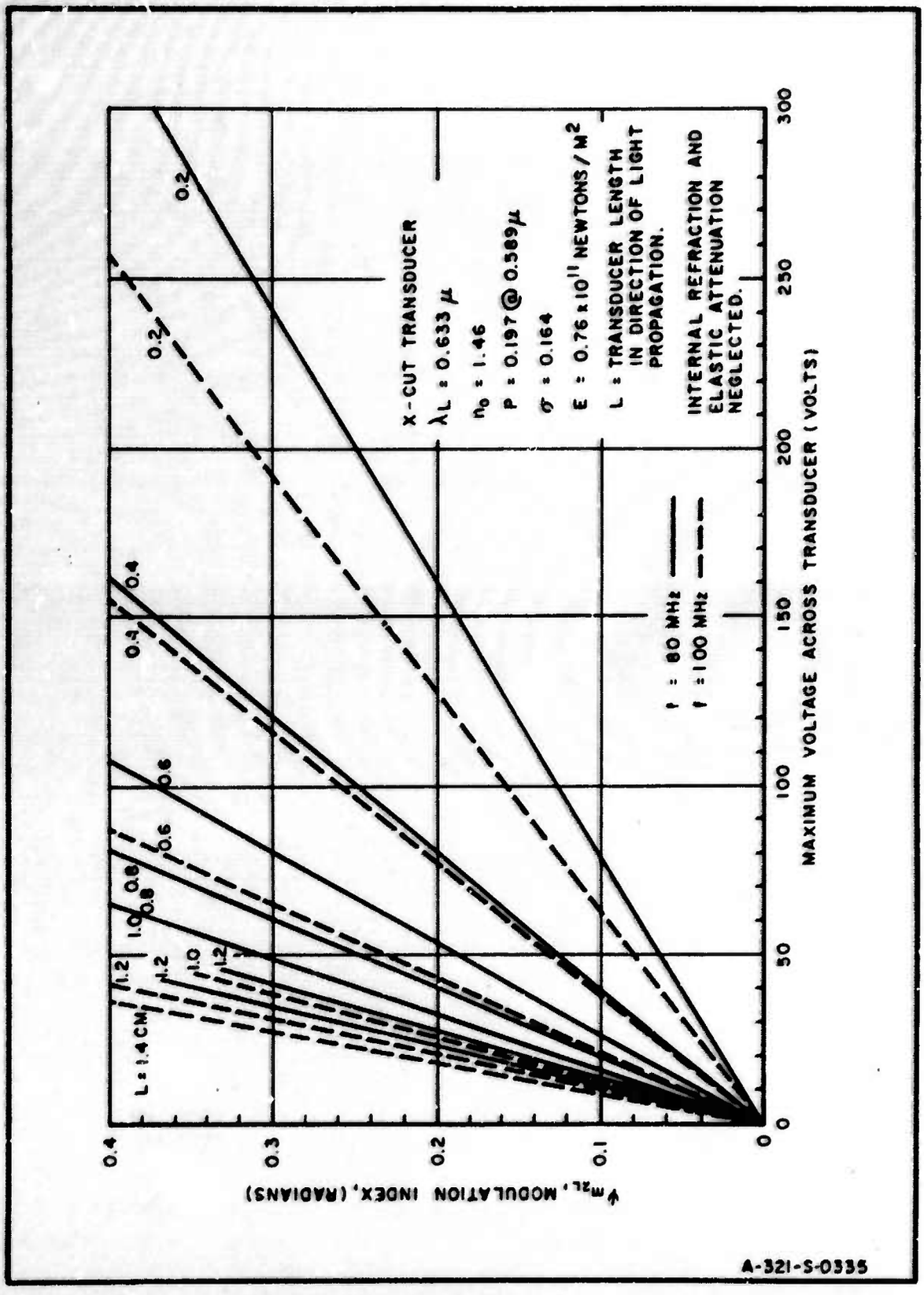

FIG.17 MODULATION INDEX VS. COMPRESSIONAL TRANSDUCER VOLTAGE WITH L AND f AS INDEPENDENT PARAMETERS

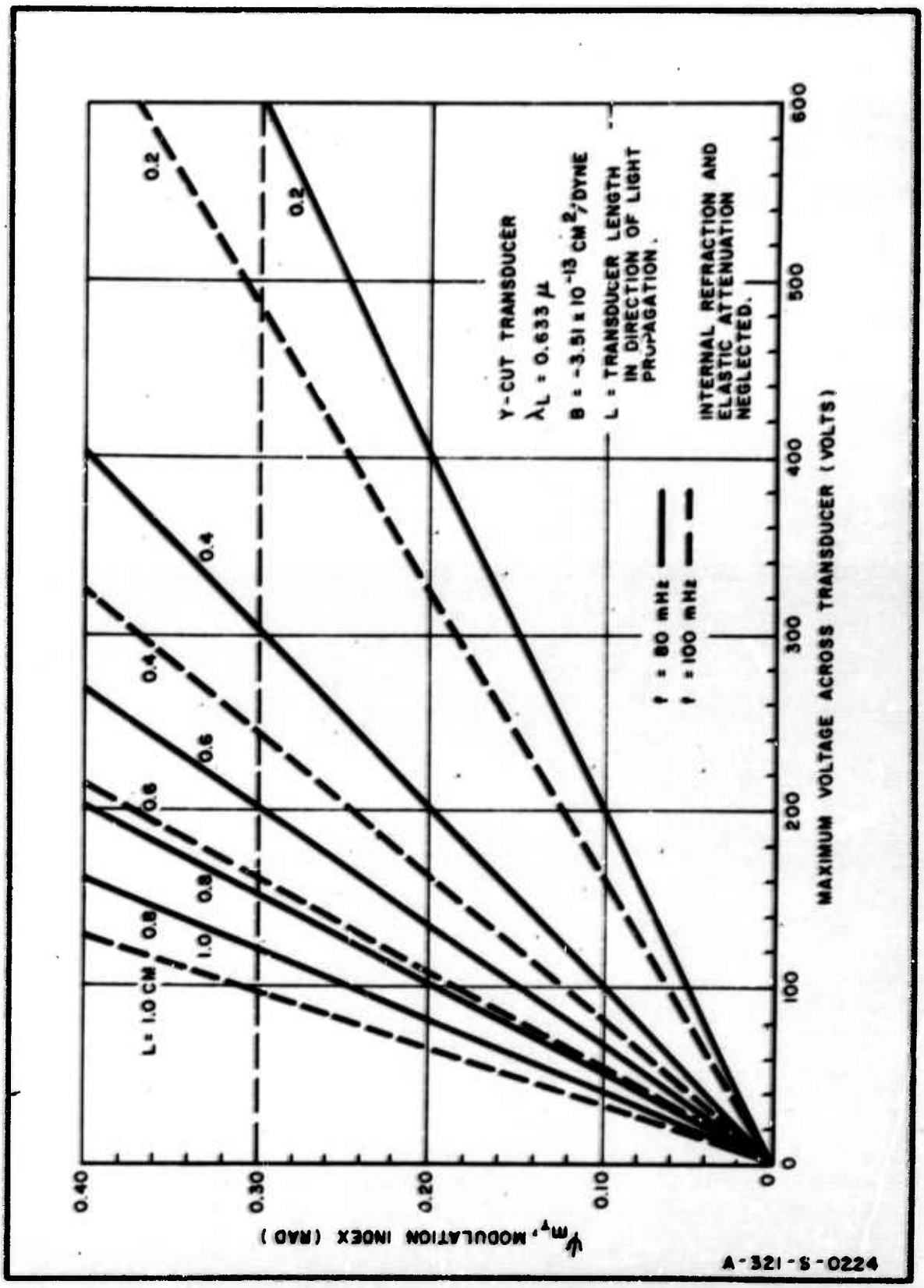

FIG. 18 MODULATION INDEX vs. SHEAR TRANSDUCER VOLTAGE WITH L AND f AS INDEPENDENT PARAMETERS.

the 2-direction, i.e., normal to the direction of propagation of the elastic waves.

It is seen that for a given modulation index, the required voltage in the L wave mode of operation is significantly less than in the T wave mode. This can be explained, theoretically, by considering Eqs. (61), (78), and (79).

From Eq. (61), the stress-optic constant is related to the Neumann strain-optic constants through the equation,

$$B = \left(\frac{1+\sigma}{E}\right) n_o^2 (q - p) = \left(\frac{1+\sigma}{E}\right) n_o^2 \left(\frac{q}{p} - 1\right) p \ .$$

Substituting the numerical values for p and q then gives

$$|B| = 0.554 \left(\frac{1+\sigma}{E}\right) n_o^2 p \ .$$

This quantity can now be compared to the corresponding quantity in the formula for $\psi_{m_{2L}}$. If

$$\bar{B}_L \equiv 2\left(\frac{1+\sigma}{E}\right) n_o^2 p \ .$$

then

$$|B| = \frac{0.554}{2} \bar{B}_L = 0.277 \, \bar{B}_L \ .$$

Hence, even though $\Phi_x < \Phi_y$, for any given values of f_o and A, the above relationship indicates that the L wave interaction will be markedly stronger than the T wave interaction.

The high voltages required to achieve the limiting modulation index, $\psi_m = 0.3$ radian, in Fig. 18 shows that the shear mode of operation is highly inefficient and, according to the power formulas in Table II, can be expected to absorb a relatively large amount of power, even when the transducer area is small.

Considerable improvement in this condition can be obtained by operating in the compressional mode where, by reference to Fig. 17, the required voltage for a given ψ_m and L is seen to be less than one-half that for the comparable shear mode.

D. INTERNAL REFRACTION EFFECTS

So far, in this study of a solid light modulator, the effect of a refractive index gradient in the elastic wave field has been neglected. As a result, it has been shown that the light is only phase-modulated after passing through the field and the diffraction can be explained by the simple Raman-Nath theory.

Actually, the existence of refractive index gradients in the sinusoidally varying elastic field will tend, through refraction, to bunch and spread apart the light rays with a periodicity equal to that of the field. Since the emerging

light intensity is directly related to the ray density, amplitude modulation will occur simultaneously with the phase modulation. If this amplitude modulation is large enough, it can adversely effect the simple relationship between the diffracted light amplitude and the modulation index. Therefore, identification of the controlling parameters is important in order to establish the necessary criteria for limiting the modulation to an acceptable level.

Analytical investigations of internal refraction effects have proceeded along two lines of approach. In one, the geometrical problem of light rays bending in a variable refractive index field has been treated. In the other, the effect of such bending on the diffraction pattern itself was of primary concern.

The former approach yields a picture of the bending over an elastic wavelength as a function of known parameters. Therefore, the extent of the bunching, for a specific set of parameter values, is made clear and a limiting criteria for simple Raman-Nath diffraction can be established.

The latter approach shows that, for normal light incidence, the intensity of the diffraction fringes, but not their form, will be affected as a result of the refraction phenomenon. A second, stronger, criterion for limiting the amplitude-modulation to an acceptable level can then be established by noting the variation in the first-order intensity from that predicted by the simple Raman-Nath theory, as the governing parameters are changed.

The geometrical theory of internal refraction derives from the work of Lucas and Bicquard.[22] Although their treatment is quite general, a solution for the trajectory equation was obtained only for the case where:

1. The index of refraction could be represented by the equation,

$$n = n_o + \delta n_m \cos \frac{2\pi}{\lambda_e} x \ .$$

2. $\delta n_m \ll n_o$

Since these conditions apply in the solid light modulator under consideration, the results obtained from their theory should be valid.

The computed light ray trajectories over an elastic wavelength, as a function of the parameter[23]

$$M = \frac{1}{\lambda_e} \sqrt{\frac{2\pi \psi_m \lambda_L L}{n_o}} \ , \qquad (82)$$

is shown in Fig. 19. The first crossing point occurs at $M = 1.57 = \frac{\pi}{2}$. The significance of this crossing point is that, if the parametric values in Eq. (82) are such that a value of $M \geq 1.57$ is obtained, the light emerging from the modulation will appear to come from a series of line sources spaced λ_e apart. Thus, the nature of the diffrac-

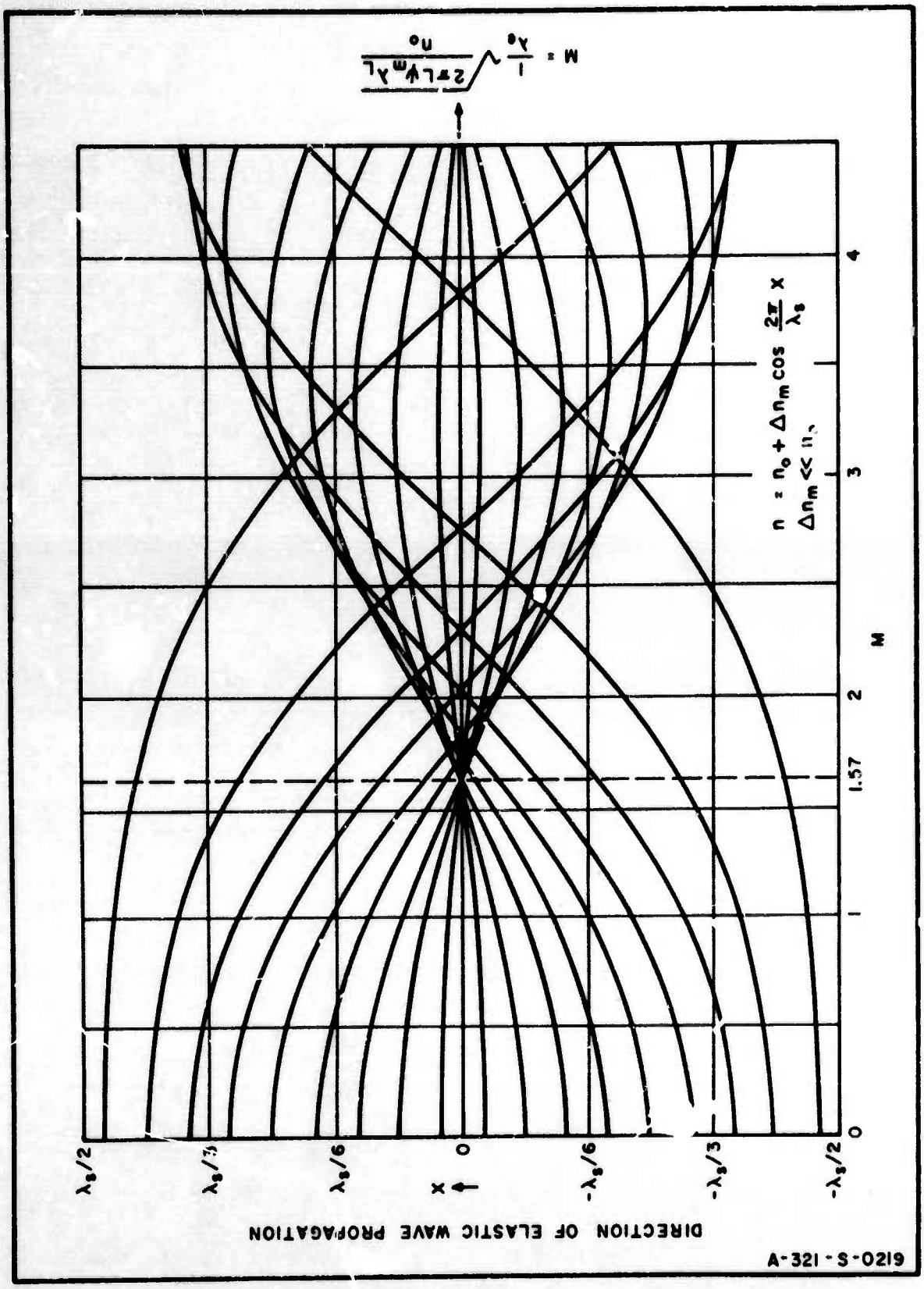

FIG. 19 LIGHT RAY TRAJECTORIES

tion will change significantly as the modulator is transformed from a pure phase grating into a line and phase grating.

If $M = 1.57$ is now considered a limiting criterion for simple Raman-Nath diffraction, the critical relationship between the modulation index and L can be determined from Eq. (82), with $M = \frac{\pi}{2}$. Hence,

$$\psi_{m_c} = \frac{\pi}{8} \frac{n_o \lambda_e^2}{L \lambda_L} \quad . \tag{83}$$

This expression is Willard's criterion[24] for simple Raman-Nath diffraction, in slightly modified form. It indicates the maximum modulation index that will still maintain the simple Raman-Nath diffraction for a given L, once the other parameter values are known.

Equation (83) is plotted in Figs. 20 and 21 for L and T wave modes of operation, respectively. In each plot, curves for the 80 and 100 MHz frequency are given.

The modification to the first-order peak intensity of the diffraction pattern due to internal refraction has been derived, in a simple way, by Rao and Murty.[25] For normally incident light and $\psi_m < 1$ their expression can be written in the form,

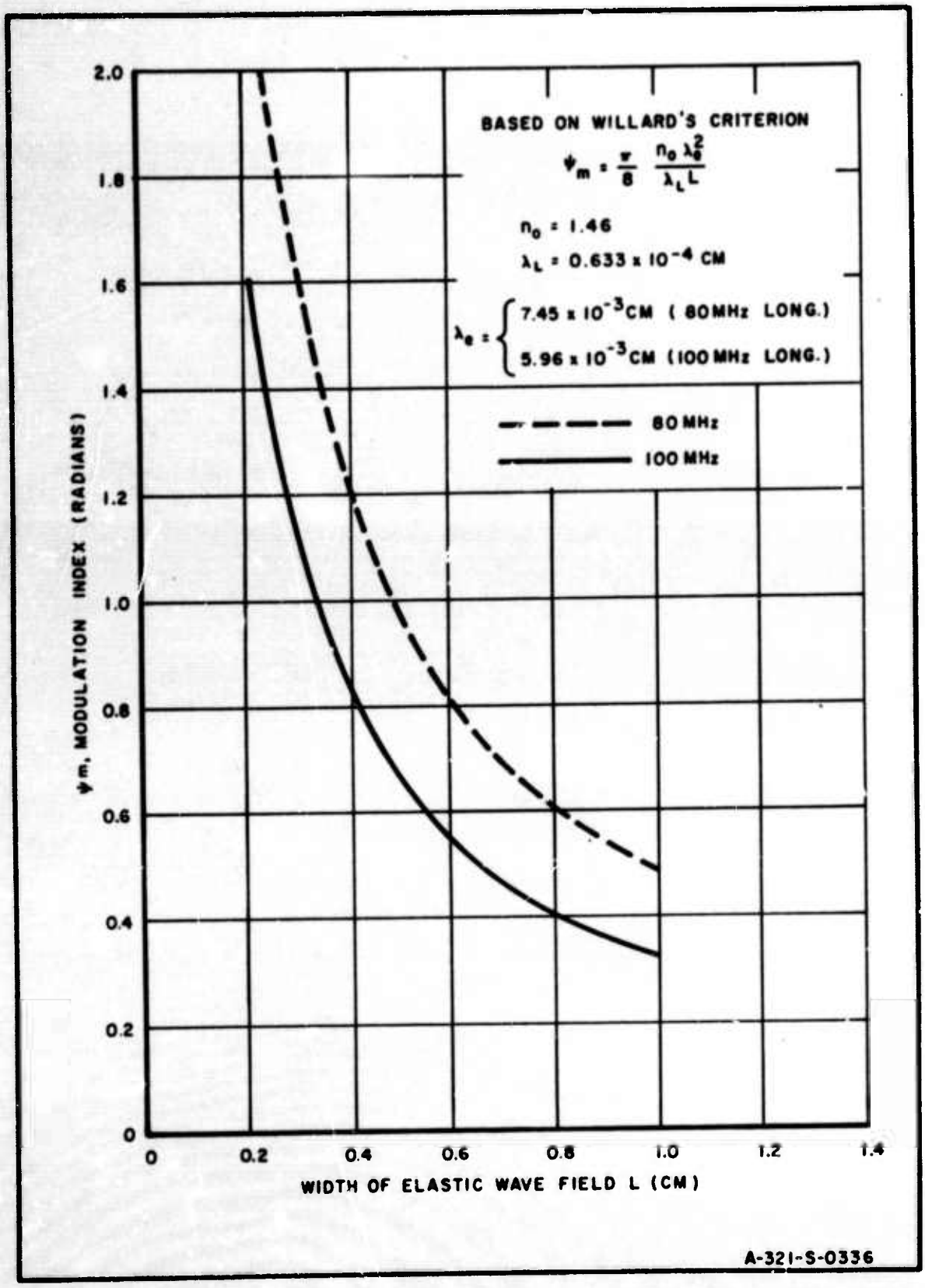

FIG. 20 LIMITING VALUES OF MODULATION INDEX FOR NORMAL DIFFRACTION VS. WIDTH OF ELASTIC WAVE FIELD L, FOR LONGITUDINAL WAVES

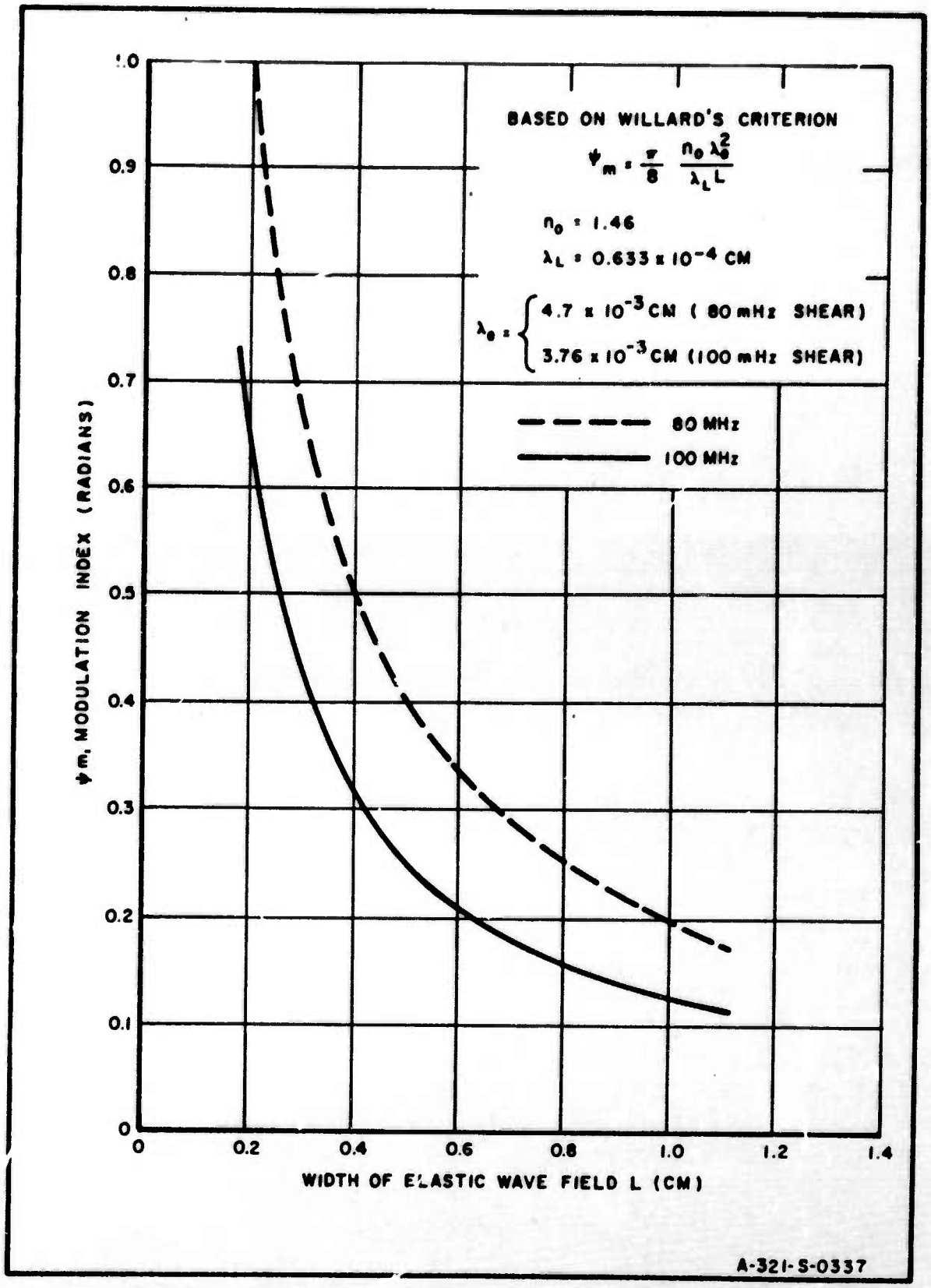

FIG. 21 LIMITING VALUES OF MODULATION INDEX FOR NORMAL DIFFRACTION VS. WIDTH OF ELASTIC WAVE FIELD L, FOR SHEAR WAVES

$$\frac{I_{1m}(\frac{L}{\lambda_e^2})}{I_{1m}(0)} = \left[\frac{\sin\frac{\pi\lambda_L L}{2n_o\lambda_e^2}}{\frac{\pi\lambda_L L}{2n_o\lambda_e^2}}\right]^2 , \tag{84}$$

provided

$$n_o\delta n_m \frac{\lambda_e^2}{\lambda_L^2} = \frac{n_o\psi_m\lambda_e^2}{2\pi\lambda_L L} \ll 1 , \tag{85}$$

where $I_{1m}(L/\lambda_e^2)$ is the maximum first-order intensity when internal refraction is taken into account, and $I_{1m}(0)$ is the intensity given by the simple Raman-Nath theory, i.e.,

$$I_{1m}(0) \simeq \frac{\psi_m^2}{4} I_{om} \tag{86}$$

when $\psi_m < 1$.

Figure 22 is a plot of $I_{1m}(L/\lambda_e^2)/I_{1m}(0)$ vs L for 80 and 100 MHz in the shear mode of operation. Note that severe reductions in the first-order intensity will occur for the larger transducers even though Willard's criterion is satisfied.

The validity of this plot can be tested by applying the most severe practical conditions to the inequality, Eq. (85). Letting $\lambda_e = 4.7 \times 10^{-3}$cm (80 MHz), L = 0.2 cm, and $\psi_m = 0.3$,

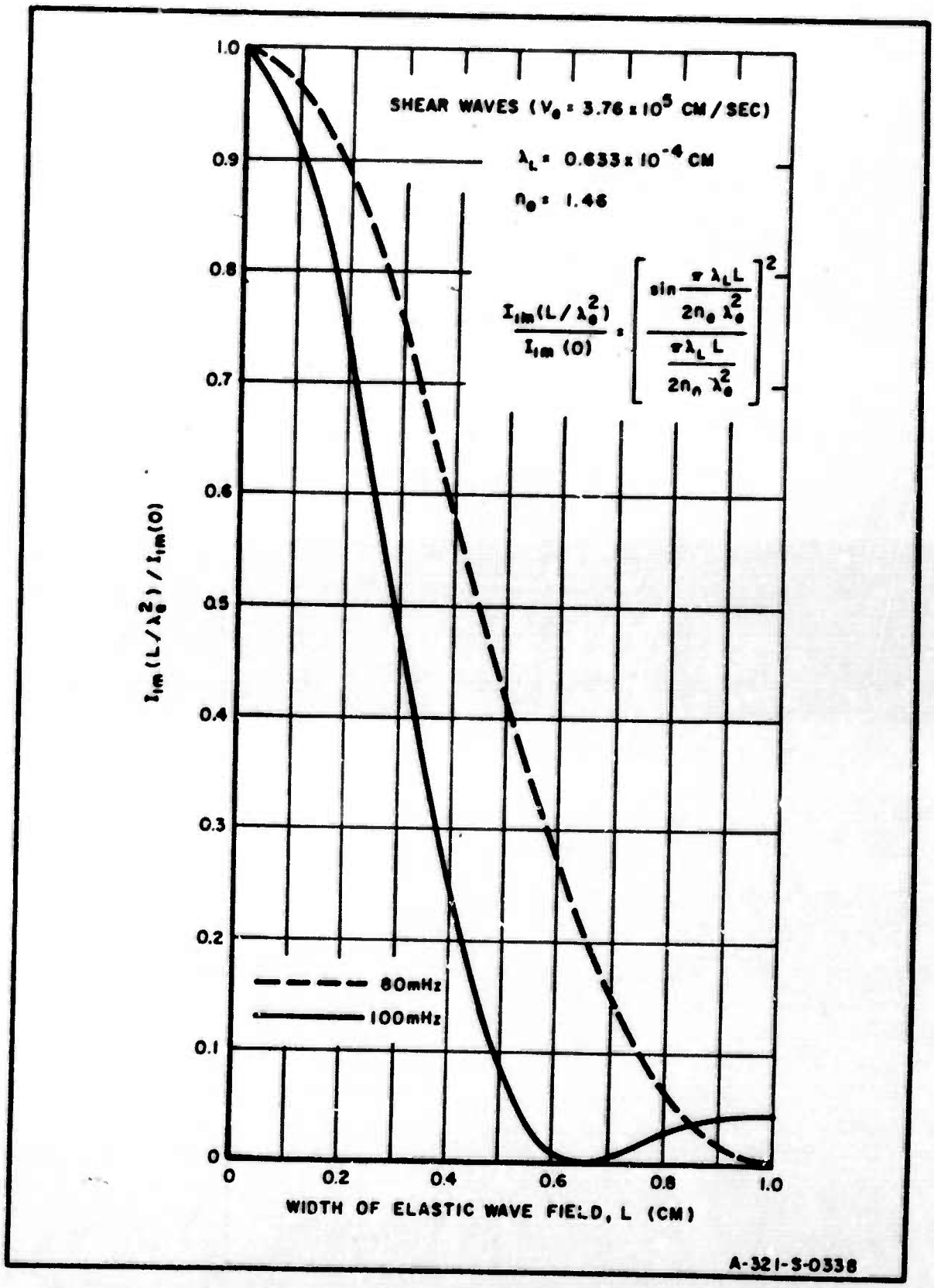

FIG. 22 FIRST-ORDER INTENSITY AFTER INTERNAL REFRACTION BY SHEAR WAVES

$$n_o \delta n_m \frac{\lambda_e^2}{\lambda_L^2} = 0.122 \ll 1 \ .$$

Hence, Eq. (84) is valid over the entire useful range of L.

The corresponding plot for the longitudinal wave mode of operation is shown in Fig. 23. It is immediately evident that a significantly smaller reduction in intensity will take place, for a given L, with this mode of operation when compared to the shear mode. It should be noted, however, that the condition, Eq. (85), is violated when $L \leq 0.2$ cm at 80 MHz. This presents no problem because, from a design viewpoint, the L wave transducers will always call for larger values of L as a result of the optimal design considerations to be discussed in the next section.

The expression for the first-order peak intensity can be written in terms of the peak intensity of the zero-order by using Eq. (86). Hence,

$$\frac{I_{1m}(\frac{L}{\lambda_e^2})}{I_{om}} = \frac{\psi_m^2}{4}\left[\frac{\sin \frac{\pi\lambda_L L}{2n_o\lambda_e^2}}{\frac{\pi\lambda_L L}{2n_o\lambda_e^2}}\right]^2 , \qquad (87)$$

where it is seen that the effect of internal refraction is to "weight" the intensity obtained from the simpler theory without changing the form of the diffraction pattern.

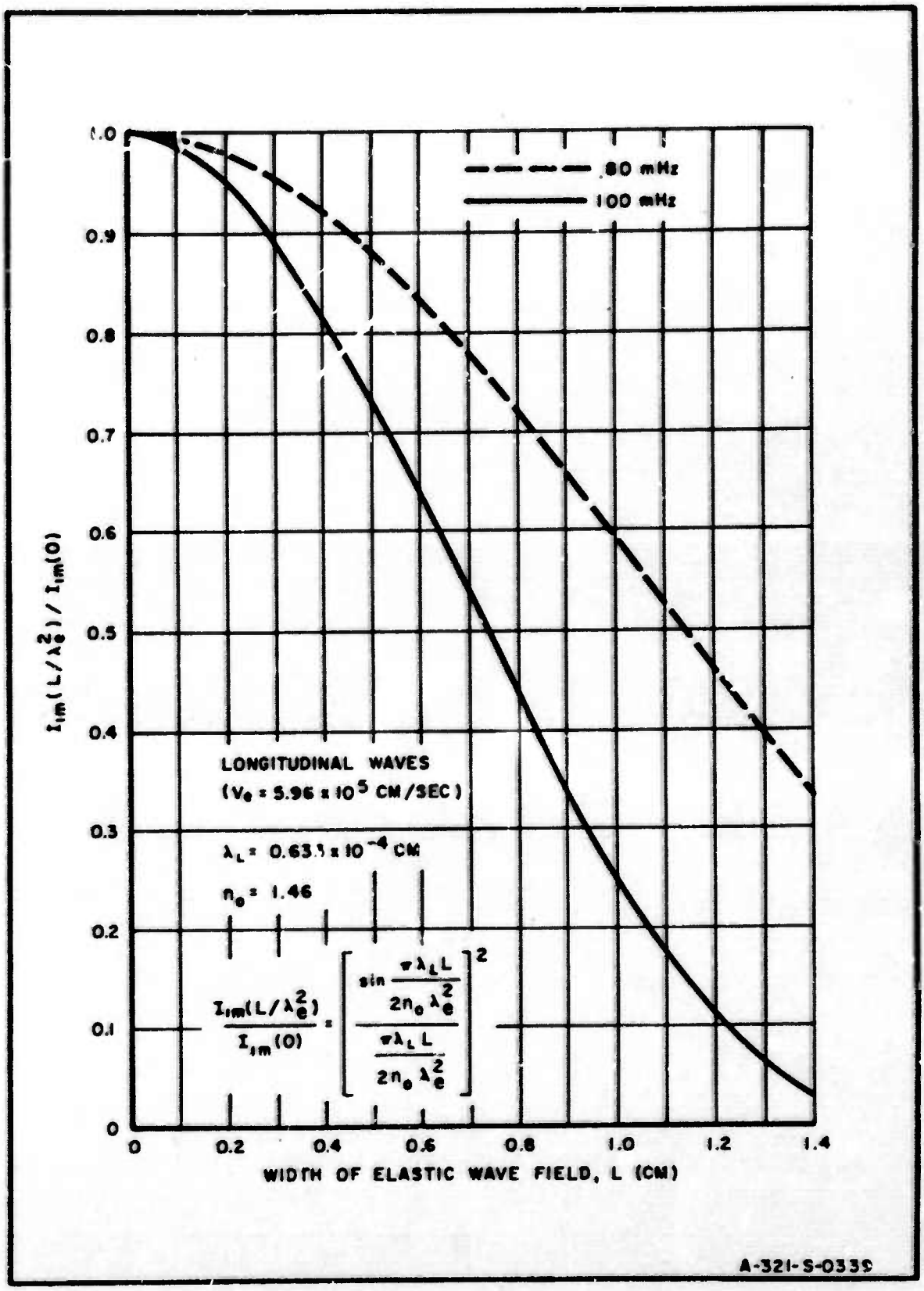

FIG. 23 FIRST-ORDER INTENSITY AFTER INTERNAL REFRACTION BY LONGITUDINAL WAVES

E. OPTIMIZATION OF THE TRANSDUCER WIDTH

The transducer width is equal to the width of the elastic wave field, L, when beam spreading is constrained by limiting the length of the elastic wave propagation in the modulator to the Fresnel region.

The effect of this parameter on the first-order peak intensity has been indicated in the previous discussion, specifically by Eqs. (62) and (87), where it is seen that increasing L will increase ψ_m but, at the same time, decrease the value of the weighting function at a faster rate. Obviously, some optimal value of L must exist for which the intensity ratio in Eq. (87) is maximized. To obtain this optimal value, consider the effective modulation index defined as

$$\bar{\psi}_m \equiv \frac{\sin \nu}{\nu} \psi_m ,$$

where

$$\nu = \frac{\pi \lambda_L L}{2 n_o \lambda_e^2} .$$

Differentiating $\bar{\psi}_m$ with respect to L and setting the derivative equal to zero gives,

$$\frac{d\bar{\psi}_m}{dL} = \left[\frac{\cos \nu}{\nu} - \frac{\sin \nu}{\nu^2}\right] \frac{d\nu}{dL} \psi_m + \frac{\sin \nu}{\nu} \frac{d\psi_m}{dL} = 0,$$

or, upon substituting for ν and ψ_m,

$$\frac{d\bar{\psi}_m}{dL} = \cos \nu = 0 .$$

Hence,

$$\nu = \frac{\pi}{2} , \frac{3\pi}{2} , \ldots .$$

Since $\nu > \pi$ would carry in ν/ν out of the main lobe, the only satisfactory solution is $\nu = \frac{\pi}{2}$. Thus,

$$L_{opt} = \frac{n_o \lambda_e^2}{\lambda_L} . \qquad (88)$$

This expression must now be tested to see that both Willard's criterion, Eq. (83), and the condition given in Eq. (85) will not be violated for modulation indices, ψ_m, $\leq$ 0.3 radian. Substituting Eq. (88) into Eq. (83), we have

$$\psi_{m_c} = \frac{\pi n_o \lambda_e^2}{8 \lambda_L L_{opt}} = \frac{\pi}{8} \simeq 0.39 \text{ radian}$$

which implies no restriction in this regard. Substituting Eq. (88) into Eq. (85) then gives,

$$\frac{\psi_m}{2\pi} \ll 1$$

as a second criterion on ψ_m. With $\psi_m = \frac{\pi}{8}$, the left side equals $\frac{1}{16}$ or $0.0625 \ll 1$. Hence, L_{opt} is a valid design parameter which will assure maximum electro-optic performance in the modulator.

No consideration has been given to elastic wave attenuation (which would supply a multiplicative factor to $\bar{\psi}_m$) because at the frequencies and optical apertures of interest the effect of this attenuation in fused-silica is negligible.[26] Also, since the attenuation factor is independent of L, it would have no effect upon the expression for L_{opt} given in Eq. (88).

The weighting function in Eqs. (84) and (87) can now be evaluated and L_{opt} determined for L and T wave modes of operation at 80 and 100 MHz. In all cases it is seen that $\sin v/v = \frac{2}{\pi} = 0.637$. Therefore,

$$W.F. = \left[\frac{\sin v}{v}\right]^2 = 0.406.$$

Referring to Figs. 22 and 23, the values of L_{opt} are then:

$$\begin{aligned} L_{opt} &= 1.3 \text{ cm (80 MHz, L mode)} \\ &= 0.83 \text{ cm (100 MHz, L mode)} \\ &= 0.5 \text{ cm (80 MHz, T mode)} \\ &= 0.33 \text{ cm (100 MHz, T mode).} \end{aligned}$$

V. REFERENCES

References 1 through 12, 20, 23 and 26 were prepared at the Electronics Research Laboratories, School of Engineering and Applied Science, Columbia University, New York, New York 10027.

1. Aimette, A., Lambert, L., Arm, M., "Electro-Optical Signal Processing Techniques for Phased Array Antennas," Progress Report P-1/199, January 1, 1964, Unclassified.

2. Aimette, A., Arm, M., Brown, D., "Electro-Optical Signal Processing Techniques for Phased Array Antennas," Progress Report P-2/199, April 1, 1964, Unclassified.

3. Aimette, A., Arm, M., Wyman, N., "Electro-Optical Signal Processing Techniques for Phased Array Antennas," Progress Report P-3/199, July 1, 1964, Unclassified.

4. Aimette, A., Arm, M., Wyman, N., "Electro-Optical Signal Processing Techniques for Phased Array Antennas," Progress Report P-4/199, October 1, 1964, Unclassified.

5. Aimette, A., Arm, M., Lambert, L., Wyman, N., "Electro-Optical Signal Processing Techniques for Phased Array Antennas," Progress Report P-1/321, January 1, 1965, Unclassified.

6. Aimette, A., Arm, M., Lambert, L., "Electro-Optical Signal Processing Techniques for Phased Array Antennas," Progress Report P-2/321, April 1, 1965, Unclassified.

7. Aimette, A., Wyman, N., "Electro-Optical Signal Processing Techniques for Phased Array Antennas," Progress Report P-3/321, July 1, 1965, Unclassified.

8. Aimette, A., Arm, M., Lambert, L., Weil, K., Wyman, N., "Electro-Optical Signal Processing Techniques for Phased Array Antennas," Progress Report P-4/321, October 1, 1965, Secret.

9. Aimette, A., Arm, M., Bernstein, S., "Electro-Optical Signal Processing Techniques for Phased Array Antennas," Progress Report P-5/321, January 1, 1966, Unclassified.

10. Aimette, A., Arm, M., Bernstein, S., Krusos, G., Minkoff, J., Wyman, N., "Electro-Optical Signal Processing Techniques for Phased Array Antennas," Progress Report P-6/321, April 1, 1966, Unclassified.

11. Arm, M., Bernstein, S., Minkoff, J., Wyman, N., "Electro-Optical Signal Processing Techniques for Phased Array Antennas," Progress Report P-7/321, July 1, 1966, Unclassified.

12. Lambert, L., "Electro-Optical Signal Processors for Array Antennas," Technical Report T-1/321, May 2, 1965, Unclassified.

13. Born, M. and Wolf, E., "Principles of Optics," 2nd ed., Pergamon Press, 1964.

14. Mueller, H., "Determination of Elasto-Optical Constants with Supersonic Waves," Zeits. f. Kristallographie, Vol. 99, 1938, pp. 121-141.

15. Courant, R., "Differential and Integral Calculus," Interscience, Vol. II, 1959, p. 188.

16. Mueller, H., "The Theory pf Photoelasticity," Journal of the American Ceramic Society, Vol. 21, 1938, p. 27.

17. Mason, W. P., "Physical Acoustics and the Properties of Solids," D. Van Nostrand Co., 1958, p. 369.

18. Sokolnikoff, I. S., "Mathematical Theory of Elasticity," 2nd ed., McGraw-Hill, 1956.

19. Konig, W. F., Lambert, L. B., Schilling, D. L., "The Bandwidth, Insertion Loss, and Reflection Coefficient of Ultrasonic Delay Lines for Backing Materials and Finite Thickness Bonds," IRE Convention Record, Part 6, Ultrasonics, 1961, pp. 285-295.

20. Konig, W. F., "Useful Constants for Ultrasonic Delay Line Calculations," Note Report N-5/152, October 15, 1959, Unpublished Internal Report.

21. Aleksandrov, K. S., Gurovits, L. S., Kamenskii, E. J., "Effect of an Intermediate Layer on the Frequency Characteristics of Ultrasonic Delay Lines," Soviet Physics-Acoustics, Vol. 6, No. 2, October-December 1960, p. 170.

22. Lucas, R. and Biquard, P., "Propriétés Optiques des Milieux Solides et Liquides Soumis aux Vibrations Élastiques Ultra Sonores," Journal de Physique, Vol. 3, No. 7, 1932.

23. Arm, M., Lambert, L., Weissman, I., "Advanced Radar Resolution Techniques - Development of a Two-Dimensional Filter," Progress Report P-2/153, January 4, 1960, Unclassified.

24. Willard, G. W., "Criteria for Normal and Abnormal Ultrasonic Light Diffraction Effects," Journal of the Acoustical Society of America, Vol. 21, No. 2, March 1949.

25. Rao, B. R. and Murty, J. S., "Diffraction of Light by Weak Ultrasonic Fields," Zeits. f. Physik., Bd. 152, 1958, p. 440.

26. Minkoff, J., "Solid Light Modulators - Choice of Optimum Mode of Propagation," Research Note N-17/321, April 1, 1966, Unpublished Internal Report.

BLANK PAGE

Security Classification

DOCUMENT CONTROL DATA - R & D

(Security classification of title, body of abstract and indexing annotation must be entered when the overall report is classified)

1. ORIGINATING ACTIVITY (Corporate author)
Electronics Research Laboratories
Columbia University

2a. REPORT SECURITY CLASSIFICATION
Unclassified

2b. GROUP

3. REPORT TITLE
Birefringence in Amorphous Solids With Application to Solid Light Modulators

4. DESCRIPTIVE NOTES (Type of report and inclusive dates)
Technical Report

5. AUTHOR(S) (First name, middle initial, last name)
S. Bernstein, J. Minkoff, M. Arm

6. REPORT DATE
January 15, 1967

7a. TOTAL NO. OF PAGES
106

7b. NO. OF REFS
26

8a. CONTRACT OR GRANT NO.
AF 49(638)-1478

b. PROJECT NO.
ARPA Order 279 Amend 5

c.
Project 7300-2837

d.

9a. ORIGINATOR'S REPORT NUMBER(S)
T-3/321

9b. OTHER REPORT NO(S) (Any other numbers that may be assigned this report)

10. DISTRIBUTION STATEMENT
(1) (2)

11. SUPPLEMENTARY NOTES

12. SPONSORING MILITARY ACTIVITY
Advanced Research Projects Agency
Air Force Office of Scientific Research

13. ABSTRACT

The theory of birefringence in a transparent, amorphous solid is developed from fundamental principles in order to obtain a design formulation for spatial light modulators that will operate at 100 MHz center frequency with at least 50 per cent bandwidth. Both longitudinal and shear wave elasto-optical interactions are treated.

Relations for the phase modulation index and the diffracted light intensity and polarization, as functions of the modulator parameters, are presented for the case of normal light incidence. The effect of internal refraction on the first-order peak intensity is then quantitatively examined. From this consideration, a criterion for obtaining maximum optical performance in the modulator is derived.

An analysis of the quartz transducers used to generate the elastic waves in the modulators is presented as an integral part of the design formulation. The effect of lead and indium bonds on transducer response is treated in detail.

DD FORM 1 NOV 68 1473

Security Classification

14. KEY WORDS	LINK A		LINK B		LINK C	
	ROLE	WT	ROLE	WT	ROLE	WT